Phototriggered proton-selective carrier currents through photoswitchable membranes

Juergen Pfeffermann[1,a], Rohit Yadav[1,a], Toma Glasnov[2], Oliver Thorn-Seshold[3], Peter Pohl[1]

[1]Institute of Biophysics, Johannes Kepler University Linz, Linz, Austria

[2]Institute of Chemistry, Karl-Franzens-University, Graz, Austria

[3]Faculty of Chemistry and Food Chemistry, Dresden University of Technology, Dresden, Germany

[a]These authors contributed equally: Juergen Pfeffermann and Rohit Yadav.

The regulation of ion transport across biological membranes using light is a powerful research tool with potential therapeutic applications. Microbial channelrhodopsins, widely used in optogenetics, enable passive photocurrents that facilitate advanced studies of synaptic plasticity and neuronal connectivity. However, their applicability is limited by the need for genetic transfection to introduce channelrhodopsins into target cells. Here, we present a synthetic alternative combining small-molecule carriers with azobenzene-containing photolipids (OptoDArG) to achieve rapid and reversible ion-selective permeability modulation by light. Incorporating a novel lipidated nile blue derivative (NB-lipid) into photoswitchable bilayers enabled fully reversible ≈200-fold on–off modulation of H^+ currents under UV and blue light illumination. The transport kinetics classify NB-lipids as cationic protonophores, demonstrating high sensitivity to OptoDArG-mediated changes in lipid packing and bilayer thickness. Another protonophore, carbonyl cyanide *m*-chlorophenylhydrazone (CCCP), exhibited similar sensitivity, though to a lesser extent. This concept extends beyond protonophores: valinomycin-mediated K^+ currents showed several-fold increases under UV light, rapidly reversed by blue light-induced generation of OptoDArG's trans photoisomer. Our approach demonstrates that rapid, non-invasive, spatially precise, and reversible light-triggered currents can be achieved without genetic modifications. This strategy, exemplified by H^+-selective currents, may be extended to other ions through tailored carrier design.

1 Introduction

The biological membrane interfaces life's smallest unit, the cell, with its surroundings. The regulated transport of ions across cellular and subcellular membranes constitutes a fundamental physiological process. Amongst others, it underlies cellular respiration, neuronal excitation, immune cell signaling and ion homeostasis. Membrane transport regulation by exogenous stimuli is of both scientific and pharmaceutical interest. To that effect, light has emerged as a desirable stimulus given the site-specific, minimally-invasive, temporally-precise and reversible manner by which it may regulate membrane ion permeability.

Typically, additional components are required to achieve selective ion currents in response to incident light. Optogenetics is a classical approach towards that end [Dei11; Kle+11]. Following early work on light-driven H^+ (bacteriorhodopsin) and Cl^- pumps (halorhodopsin), later work focused on membrane-embedded microbial channelrhodopsins (ChRs) that conduct ions upon irradiance with a certain wavelength [Ern+14]; like other ion channels, ChRs can exhibit intricate gating behaviors [HN13]. Using ChRs, cation-selective currents can be generated at the millisecond timescale which achieves membrane depolarization [Boy+05]. The optogenetic approach has been most prominently used in neurophysiology in studies on synaptic plasticity and neuronal connectivity [Zha+07; HN13]. Over roughly two decades, ChR mutants with specific selectivities and gating behaviors have been created and thoroughly investigated. Yet, microbial ChRs are not native to human cells and thus transfection with genetic material is required to introduce them to their cellular and subcellular membranes.

Circumventing the requirement for delivering genetic material, progress has been made over the last decade in the field of photopharmacology which aims to regulate drug activity by light [HMT18; VSF14]. Most research there focuses on classical orthosteric or allosteric ligands to gate protein activity (e.g. ion channels and other membrane transporters) [Mül+24; Bau+24]. Yet, light can be a far more versatile tool at regulating ion transport as studies on the optocapacitive mechanism have demonstrated [Sha+12; Car+15]. The latter relies on rapid changes in bilayer capacitance that evoke depolarizing optocapacitive currents. Recently, we have demonstrated that azobenzene-containing photolipids which toggle between two conformations depending on illumination can achieve optocapacitive neuronal regulation, including the generation of action potentials [Bas+24]. Owing to their beneficial photophysical (high absorption cross section and quantum yield of photoisomerization), photochemical (low phototoxicity) and chemical properties, azobenzene moieties are exquisitely suited for endowing photosensitivity to small molecules intended for usage in the biological system [HMT18; VSF14]. With regard to membrane protein regulation, photolipids can function in two conceptually different ways: On the one hand, photolipids can act as reversible lock-and-key regulators of membrane protein function [Lic+18; Fra+16b; Mül+22]. On the other hand, photolipid photoisomerization alters material properties of the host lipid bilayer [Per+17; Pfe+21; Urb+18; Ale+23; Obe+22] and may thus gate mechanosensitive or mechanically-modulated membrane proteins [Phi+09; Pfe+21; Cre+22]. That is, with regard to the regulation of membrane ion permeability, photolipid-dependent alterations in bilayer material properties eventually allow photomechanical or optocapacitive regulation of ion channels.

Besides channels, selective ion transport may also be mediated by mobile carriers, such as hydrophobic ionophores, which facilitate ion movement across membranes [Läu72]. Indeed, a plethora of research focuses on "molecular machines" for controlling transmembrane ion transport" [Joh23] where light-dependent currents are generated and the ionophores *per se* are modified with light-sensitive moieties. Yet, "few of these membrane-active synthetic molecules are taking the leap from model bilayer membrane to cells" [RT21]. Molecular motors, another type of molecular machines, have been reported to increase membrane ion permeability upon irradiation [Gar+17]

but this has actually been shown to occur through irreversible photodynamic membrane lipid peroxidation rather than drilling [Fir+23]. Carriers can achieve high selectivity [RH74; Leb71], rivaling or surpassing ChRs in regulating specific ion gradients and avoiding cross-ion interference. However, in contrast to ChRs, classical and widely-adopted carriers are typically not rapidly modulated in their activity but specifically increase membrane background permeability to certain ions, e.g., to achieve uncoupling in mitochondria [Ant+11; Žun+21].

Here, we present a general mechanism for achieving light-dependent, millisecond-scale regulation of highly-selective carriers (Figure 1d). Inspired by research that demonstrates the pronounced dependence of ionophore transport on membrane structure [Ben+73; BFL77; KES71], we hypothesized that photolipid-mediated bilayer changes may regulate ion-selective carrier transport. Our approach leverages previous findings that the photolipid OptoDArG (Figure 1b) undergoes rapid (millisecond-scale) isomerization under intense UV (375 nm) or blue (488 nm) light, altering properties of the embedding bilayer membrane [Bas+24] (schematically shown in Figure 1c). One of those properties is membrane capacitance, C_m, which changes with bilayer hydrophobic thickness, d_ϵ, which in turn depends on which photoisomer is predominantly present. Hence, the photoswitchable bilayer can be considered to be in a trans or cis photostationary state:

$$C_\mathrm{m} = \epsilon_\mathrm{r}\,\epsilon_0 \cdot A_\mathrm{m}/d_\epsilon \tag{1}$$

where ϵ_0 is vacuum permittivity, ϵ_r relative permittivity of the bilayer and A_m bilayer surface area.

Bilayer properties and carrier-mediated ion currents may change at a rate dictated by the transition rate between the photostationary states. For the number of membrane-embedded photoisomers, $n(t)$, we can write [Bas+24]:

$$n(t) = n_0 \cdot \exp(-k\,E_\mathrm{e}\,t) \tag{2}$$

where n_0 is initial photoisomer number, E_e irradiance, k irradiance-independent rate of photoisomerization, and t time after light onset. With $1\ \mathrm{cm^2\,W^{-1}\,s^{-1}} < k < 10\ \mathrm{cm^2\,W^{-1}\,s^{-1}}$ for azobenzene-containing surfactants [Ary+20] and E_e of several-hundred $\mathrm{W\,cm^{-2}}$, the global shift in bilayer material properties takes milliseconds and is readily reversible [Bas+24].

To test our hypothesis that light-mediated bilayer changes regulate carrier-induced membrane permeability, we conducted voltage-clamp current recordings using a photoswitchable planar lipid bilayer system with UV (375 nm) and blue (488 nm) laser illumination [Bas+24]. Initial experiments with valinomycin (K^+ ionophore) and CCCP (protonophore; uncoupler of oxidative phosphorylation) (Figure 1d) revealed rapid, reversible changes in selective carrier currents modulated by photolipids. We then identified a lipidated nile blue derivative (NB-lipid) that enabled effective on–off modulation of H^+-selective currents under alternating UV and blue light in photoswitchable bilayers. Our findings highlight bilayer mechanics as critical for carrier current modulation and suggest that tailored carrier design, considering bilayer sensitivity and desired ion selectivity, may enable light-based regulation of ion transport. This approach holds potential for application in both biological and synthetic cells.

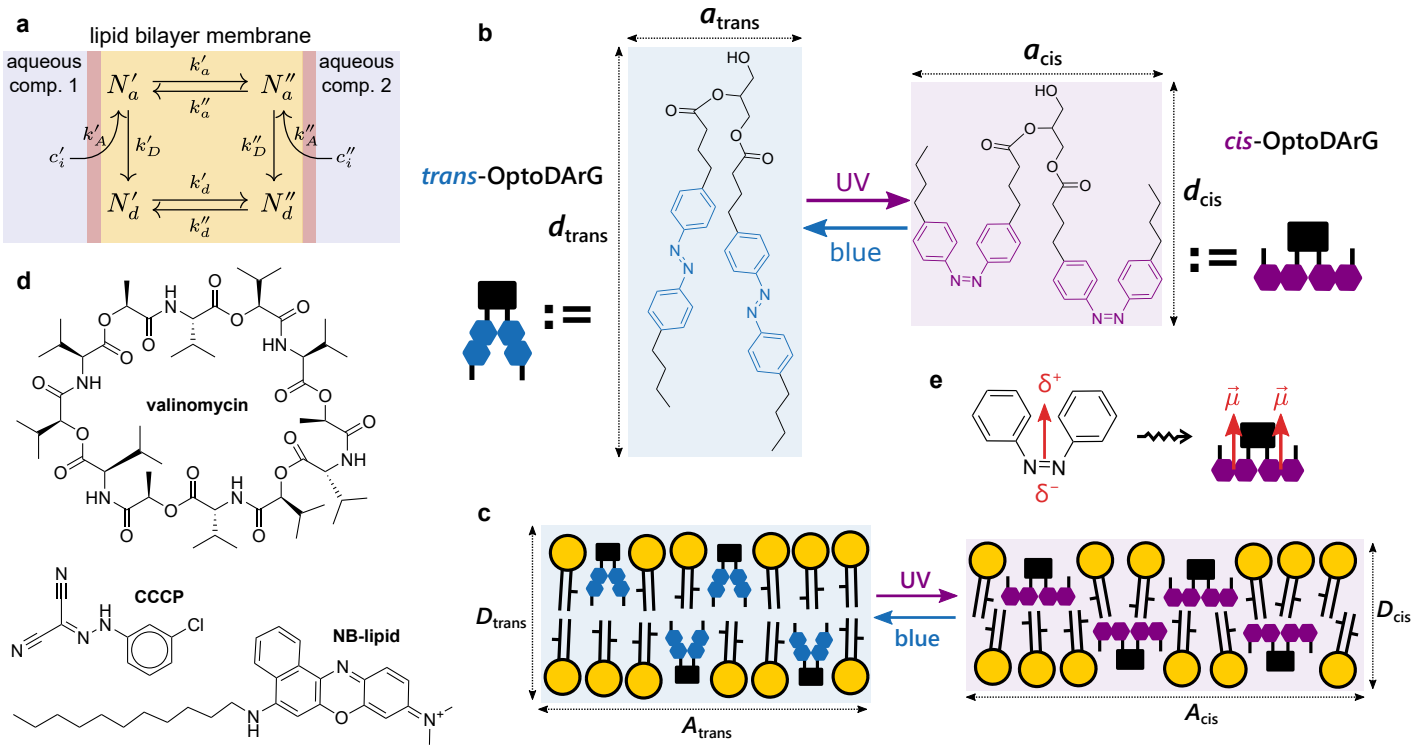

Figure 1: a, A basic scheme of carrier-mediated transmembrane ion transport that applies to both cationic and anionic ionophores/protonophores (the symbols are described in Section S2). Briefly, to traverse the lipid bilayer membrane from aqueous compartment 1 to 2, an ion present at concentration c_i' associates with an interfacially-adsorbed ion-dissociated carrier present at concentration N_d'; k_A' denotes the association rate constant at side 1. The resulting adsorbed carrier–ion complex (concentration denoted N_a') translocates across the membrane at a rate k_a'. At interface 2, the ion may be released from the carrier–ion complex (the corresponding dissociation rate constant is k_D'), resulting in the carrier-mediated translocation of a single ion. The resulting ion-dissociated carrier is free to recycle to side 1; the corresponding rate constant is k_d'' for movement from interface 2 to 1. **b,** The photolipid OptoDArG in its trans and cis state: blue light (488 nm) generates mainly the former, UV light (375 nm) generates mainly the latter, but for brevity the photoequilibria will henceforth be indicated as simply "trans" (blue light) and "cis" (UV light). cis-OptoDArG is broader ($a_{cis} > a_{trans}$) and shorter ($d_{cis} < d_{trans}$) than trans-OptoDArG. **c,** Both photoisomers incorporate into lipid bilayers and cellular membranes. Photoisomerization of membrane-embedded photolipids causes changes in global material properties owing to changes in molecular structure (see panel **b**). Amongst others, photoisomerization to cis-OptoDArG by UV light increases A_{m} ($A_{cis} > A_{trans}$) but reduces d_{m} ($D_{cis} < D_{trans}$), reflected in higher electrical capacitance. **d,** Chemical structures of the ion-transporting compounds used in this study: the cationic K^+ ionophore valinomycin, the anionic protonophore CCCP and NB-lipid, a lipidated nile blue derivative which behaves like a cationic protonophore. **e,** Cis-azobenzene has a dipole moment, $\vec{\mu}$, of magnitude 3 D pointing in the indicated direction; δ^- and δ^+ indicate negative and positive partial charge. A simplified view of the orientation of cis-OptoDArG in the lipid bilayer (see panel **c**), where, on average, the azobenzene moieties' dipole moments point towards the interfaces. This could result in a lowering of the membrane-intrinsic positive dipole potential, Φ_{d}.

2 Results

2.1 Photolipid-based regulation of the classic K^+ ionophore valinomycin

Valinomycin, an electrically neutral dodecadepsipetide macrocyclic molecule (Figure 1d) naturally synthesized by *Streptomyces fulvissimus* [BS55], binds K^+ with a stability/association constant 10^3–10^4 times higher than that for binding Na^+ [RH74]. Both, valinomycin and the valinomycin–K^+ complex are membrane-permeable [Läu72; HLF95], enabling valinomycin to functions as a selective K^+ carrier, shuttling K^+ along its electrochemical gradient across biological membranes [Läu72].

As expected, upon adding 10 µM valinomycin to the aqueous compartments on both sides of a photoswitchable

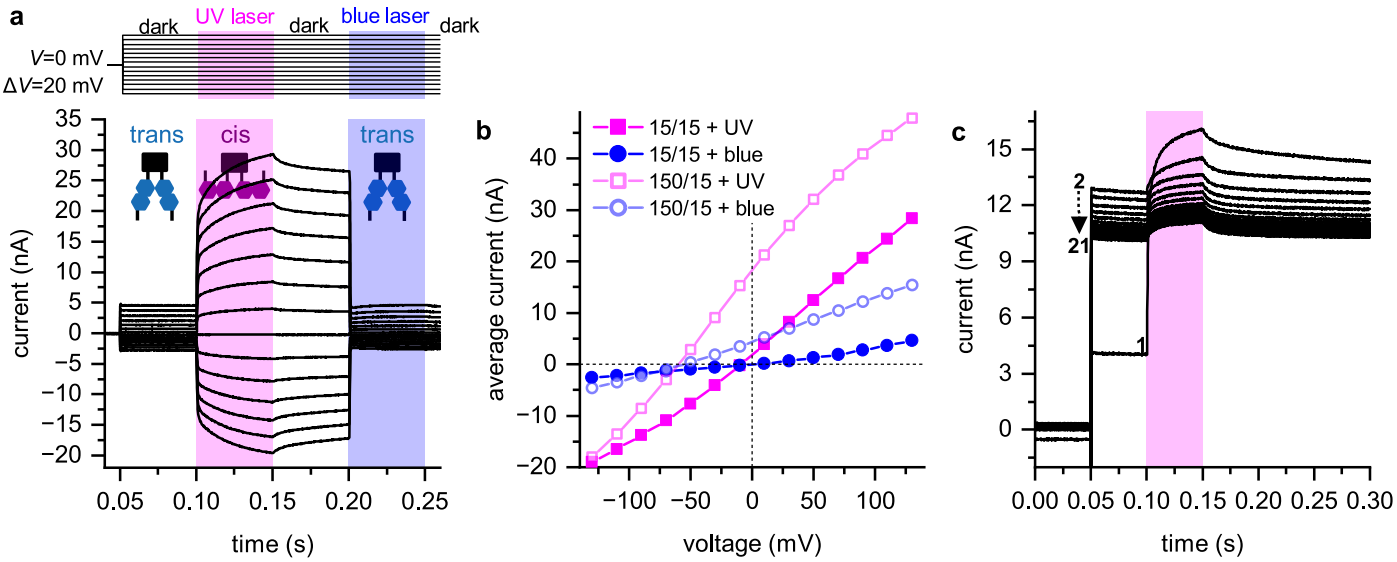

Figure 2: a, Voltage-clamp current, I, recordings on a 70 µm-diameter photoswitchable planar lipid bilayer (PLB) folded from *E. coli* PLE + 20 m% OptoDArG with 10 µM valinomycin added to the aqueous compartments (15 mM KCl, 10 mM HEPES pH 7.4) on both sides. Between 0 and 50 ms, $V = 0$ mV and between 50 and 300 ms, $V = 130$ mV to -130 mV with $\Delta V = -20$ mV; the intersweep delay was 1 s. The PLB was exposed to UV light between 100 and 150 ms and to blue light between 200 and 250 ms. Prior to starting the record, the PLB was exposed to blue light to establish the trans photostationary state. **b,** I/V curves constructed from different intervals of current traces recorded as in panel **a** at symmetric ($c_i' = c_i'' = 15$ mM KCl) and asymmetric ($c_i' = 150$ mM KCl, $c_i'' = 15$ mM KCl) ionic conditions. I_{UV} was calculated by averaging I between 125 and 150 ms (magenta square symbols); I_{blue} by averaging I between 225 and 250 ms (blue circular symbols). **c,** 80 µm-diameter photoswitchable PLB, 10 µM valinomycin in 15 mM KCl, 10 mM HEPES pH 7.4. Prior to starting the record, the PLB was exposed to blue light. The following was repeated 21 times with an intersweep delay of 1 s: Between 0 and 50 ms, $V = 0$ mV and between 50 and 300 ms, $V = 130$ mV; between 100 and 150 ms the PLB was exposed to UV light (no blue light exposure).

planar lipid bilayer (PLB), current measured under voltage-clamp conditions, I, increased from pA to several nA at $V = 130$ mV (Figure 2a). Between 0 and 50 ms, $V = 0$ mV and because K^+ concentration was symmetrical no net current flowed due to the absence of an electrochemical driving force. In the interval between 0 and 100 ms, the membrane-embedded photolipid OptoDArG was in its trans state which (i) is favored thermodynamically over the metastable cis state and (ii) can be achieved by blue light illumination [HMT18]. Consistent with its function as a K^+ ionophore, I was selective for K^+: Upon increasing $[K^+]$ at side 1 of the PLB to $c_i' = 150$ mM (c_i'' remained at 15 mM KCl), the reversal potential, V_{r}, of the constructed current–voltage (I/V) relationship (open circles in Figure 2b) shifted towards negative values ($V = \Phi_1 - \Phi_2$ is the difference in electrostatic potential between side 1, Φ_1, and side 2, Φ_2, of the PLB). By interpolation we find $V_{\mathrm{r}} = -55.9$ mV which is close to -59 mV anticipated from the Nernst equation:

$$V_{\mathrm{r}} = \ln 10 \cdot \frac{RT}{zF} \cdot \log_{10} \frac{c_i''}{c_i'} \tag{3}$$

where $\ln 10 \cdot RT/zF = 59$ mV at 25 °C. This result agrees with valinomycin as a highly-selective K^+ carrier, shuttling K^+ along its electrochemical gradient [Läu72; RH74]. The presence of trans-OptoDArG does not interfere. Critically, membrane resistance was not effectively modulated by light exposure. As detailed in Section S1, background membrane ion permeability of photoswitchable PLBs in the absence of carriers can be confidently disregarded for the purposes of this study.

At $t = 100$ ms, the bilayer was exposed to UV light for 50 ms (Figure 2a). Immediately, I increased at seemingly two different rates, one considerably faster than the other. We approximated $I(t)$ by a double-exponential model

of the form

$$I(t) = I_0 + \Delta I_1 \cdot (1 - \exp(-t/\tau_1)) + \Delta I_2 \cdot (1 - \exp(-t/\tau_2)) \tag{4}$$

where I_0 denotes basal current in the trans photostationary state (t from 50 to 100 ms), ΔI_1 and ΔI_2 the increment in I associated with growth at rate $1/\tau_1$ and $1/\tau_2$. A global fit of the current traces in Figure 2a for t from 100 to 150 ms and $|V| > 10$ mV yielded $\tau_1 = 0.36$ ms and $\tau_2 = 20.2$ ms. The fold-change in I upon UV light exposure, $I_{\mathrm{UV}}/I_{\mathrm{blue}}$, calculated from average I reached upon quantitative photoisomerization to the cis state (I_{UV}, t from 125 to 150 ms, cis photostationary state achieved by UV light exposure) and I obtained following quantitative photoisomerization back to the trans state (I_{blue}, t from 225 to 250 ms, trans photostationary state achieved by blue light exposure), is 8.0 ± 1.9 (mean±SD). At the same time, selectivity for K^+ was retained: $V_{\mathrm{r}} = -59.7$ mV (determined by interpolation of the open squares in Figure 2b). That is, UV light which generates cis-OptoDArG causes a rapid increase in selective carrier current.

To infer whether I_{UV} was due to (i) UV light *per se* or (ii) the ensuing photolipid structural change, we conducted experiments on PLBs without OptoDArG. Thereby, we found that a noticeable fast increase in I is absent and $I_{\mathrm{UV}}/I_{\mathrm{blue}}$ calculated to merely 1.16 ± 0.002 (Figure S5a). Likewise, in experiments where we exposed photoswitchable PLBs repeatedly to UV light without intermittent blue light (Figure 2c), the large-amplitude fast increase in I was absent as well. That is, UV light exposure leads to a rapid increase in I only in the presence of trans-OptoDArG, indicating that it is a consequence of the photolipid structural change. Further, we showed that contributions from photodynamic modifications of bilayer structure upon UV light exposure played no decisive role (described in Section S3).

Critically, the increment in I due to UV light was rapidly abrogated upon blue light exposure starting at $t = 200$ ms in Figure 2a: blue light leads to a sudden drop in I back to the pre-UV-illumination current level. This happens at a rate of ≈ 7000 s^{-1} (determined by fitting a single exponential to the decay, i.e., Equation 4 with $\Delta I_2 = 0$). Considering this rapid light-induced reversibility, we conclude that the majority of I_{UV} is a result of the rapid change in photoisomer state and the ensuing changes to bilayer material properties. This is supported by the permanence of the UV light-evoked current increment without blue light exposure: in this case, I remains high, as shown in Figure 2c.

Clearly, upon turning-off the UV laser at $t = 150$ ms in Figure 2a, some current decayed spontaneously until I_{UV} was quantitatively switched-off by blue light at $t = 200$ ms. There are two components to this decay:

1. One component of the UV light-evoked current decays following each UV light pulse, clearly evident in Figure 2c. A similar current is also observed in the absence of the photolipid (Figure S5a). We cautiously attribute it to mild changes in membrane temperature during and after UV light exposure. Small changes in valinomycin-mediated K^+ conductance with temperature in liquid-state bilayers have been observed earlier [KES71]. Consistent with a temperature effect, a small increase in I is also observed upon blue light exposure (interval between 200 and 250 ms) in the presence (Figure 3a) and absence of OptoDArG (Figure S5a).

2. A second component of the UV light-evoked current decays much slower (note the intersweep delay of 1 s in Figure 2c) but eventually converges to a value around 10 nA. Consistent with a dependence of I on bilayer material properties, this component may be due to global changes in PLB constitution, e.g., a slow adaptation of the anchoring solvent annulus [Whi72] to the cis-OptoDArG-containing PLB. Indeed, a slow relaxation in the range of several seconds following UV light exposure was also observed in capacitance recordings (cf. Figure 2ab in [Bas+24]).

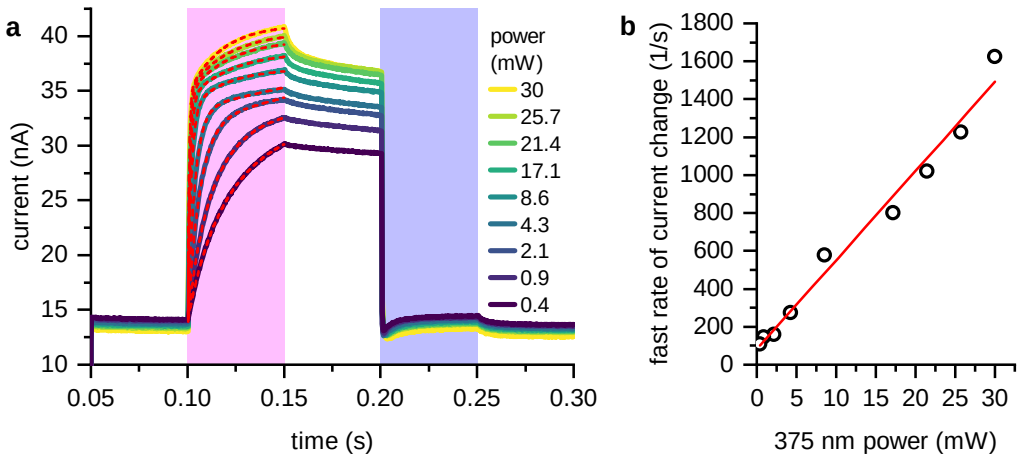

Figure 3: a, Irradiance-dependence of the UV light-triggered increment in I with valinomycin. 70 µm-diameter photoswitchable PLB folded from *E. coli* PLE + 20 m% OptoDArG with 10 µM valinomycin in 150/15 mM KCl, 10 mM HEPES pH 7.4. Recordings were conducted as in Figure 2a but with V constant at +130 mV whilst the power of the UV laser at the sample stage was varied in consecutive sweeps. The red-dashed lines are fits of the underlying data to Equation 4. **b,** Plot of k_1, the faster rate of change of I, fitted in panel **a** over respective incident UV laser power. The red line is a fit to a linear model with offset ($R^2 = 0.98$).

In any case, the majority of the UV light-evoked increment in I does not relax but remains. This is consistent with a persistent change in bilayer material properties due to the presence of cis-OptoDArG.

Upon attributing the increase in I upon UV light exposure to photolipid photoisomerization, we reasoned that the associated rate of increase in I, $k_1 = 1/\tau_1$, should be dependent on irradiance, E_e, as is the rate of photoisomerization [Bas+24]. To that effect, we conducted voltage-clamp current recordings as in Figure 2a at constant $V = 130$ mV but varied UV laser power – the result is shown in Figure 3a (because the laser profile remained unchanged, power is proportional to E_e). $I(t)$ for t from 100 to 150 ms was fit with Equation 4 (red dashed curves in Figure 3a). The fit k_1 values are linearly dependent on UV power (Figure 3b), which provides an additional argument that photolipid photoisomerization triggers changes in I. We note that the rates in Figure 3b are considerably higher than those for capacitance change observed previously [Bas+24]. That is, upon UV light exposure, I appears to change at a faster rate than membrane capacitance. Irrespective of this observation which may be assessed in detail in a separate study, the rapid reversibility of the UV light-evoked current increment upon blue light exposure suffices at evidencing the critical role of photolipid photoisomerization for the observed increase in selective carrier current.

2.1.1 On a mechanical mechanism of valinomycin current photo-modulation

Our hypothesis and observations that valinomycin activity is gated by photolipid-mediated changes in bilayer material properties are supported by earlier studies which investigated the relationship between membrane composition and valinomycin currents. Benz *et al.* [Ben+73] found that shortening lipid acyl chain length leads to an increase in k_A, the rate constant of valinomycin–K^+ association at the interface. In a later study, Benz, Fröhlich, and Läuger [BFL77] observed that increasing the degree of unsaturation in C_{20} acyl chains from one to four double bonds resulted in 7- and 24-fold increases in the translocation rates of the free carrier and the charged carrier complex, respectively. This amplification of valinomycin transport was attributed to increased membrane fluidity. However, the observed effects are unlikely to result solely from increased transversal valinomycin diffusivity. Instead, increased local partition coefficients likely play a more significant role [Zoc+13]. This model aligns with the correlation between water permeability and the area per lipid [Nag+08], specifically the increase

in water permeability with lipid unsaturation [Olb+00], which quantitatively matches the behavior of the free carrier [BFL77]. We propose that in addition to changes in fluidity, photoisomerization of membrane-embedded OptoDArG from trans to cis also affects lipid spacing (Figure 1d), thereby providing a plausible explanation for the several-fold increase in valinomycin current observed in our experiments.

2.2 Photolipid-based regulation of the weak acid protonophore CCCP

Different from valinomycin, carbonyl cyanide *m*-chlorophenylhydrazone (CCCP) is a weak acid with a pK_a around 5.9 [KBM84] to 6.1 [Leb71]. The protonated acid (AH) and negatively-charged deprotonated conjugate base (A^-) form of CCCP have similar membrane adsorption coefficients and are both membrane-permeable, rendering CCCP an effective anionic protonophore [Leb71; KBM84; OH83]. This is in contrast to other weak acids (e.g., ascorbic acid) which have very low A^- permeability [HP18]. As is usual for weak acid uncouplers [Rok+13], the considerable permeability of the A^- form of CCCP results from electron delocalization which reduces charge density. With regard to the kinetic scheme in Figure 1a and in contrast to valinomycin, the ion-dissociated (deprotonated) conjugate base, $CCCP^-$, is the charged species permeating the membrane. Conceivably, the transport rate for the AH form, $k_a = 12\,000\ \mathrm{s}^{-1}$, exceeds that of $CCCP^-$, $k_d = 175\ \mathrm{s}^{-1}$ [KBM84]. The interfacial reaction rates $k_A \cdot [H^+]$ and k_D are much larger than the transport rates and are thus effectively in equilibrium [KBM84; BM83]. Consequently, the protonophore CCCP shows Nernstian behavior for pH ≤ 9 (cf. Equation 3) [KBM84; OH83]. Like valinomycin, CCCP is used in fundamental research for conducting vesicle-based ion permeability measurements where it can effectively clamp the membrane potential (e.g., in [MM22]) or allow estimation of the fraction of vesicles without a functionally-reconstituted proton channel (as in [Boy+23]). In cell experiments, CCCP is used as an effective uncoupler of oxidative phosphorylation [HP62].

To investigate photomodulation of CCCP current, we folded a photoswitchable PLB and added 10 µM CCCP to both compartments; this concentration ensures that background proton currents contribute negligibly [OH83]. As before, I increased to several nA at $V = 130$ mV with OptoDArG in its trans state (t between 50 and 100 ms in Figure 4a). In contrast to valinomycin, I was selective for protons: in a nominal 100-fold $[H^+]$ gradient (pH 5 on side 1 and pH 7 on side 2), V_r shifted to large negative values (blue open circles in Figure 4b), in qualitative agreement with the expected $V_r = -118$ mV. Notably, the pH gradient was established by the addition of concentrated HCl to compartment 1, whereby the required acid volume was determined separately at a pH meter. Since pH 5 is outside the pH range where HEPES ($pK_a = 7.48$ at 25°C [Goo+66]) buffers effectively (i.e., $pK_a \pm 1$) and the small volume of compartment 1 is susceptible to variations, an exact agreement between experimentally-determined and theoretical V_r could not be expected. Hence, we confirmed that CCCP continues to work as a selective protonophore in photoswitchable PLBs.

As with valinomycin, we triggered the UV laser at $t = 100$ ms, causing sudden trans to cis photoisomerization. Again, this led to an increase in I (Figure 4a and closed squares in Figure 4b). I_{UV} remained selective for H^+, indicated by the retention of a large negative V_r in a nominal 2 unit pH gradient (open squares in Figure 4b). As before, I appears to increase at two different rates. A global fit of $I(t)$ for t from 100 to 150 ms and $|V| > 30$ mV with Equation 4 results in $\tau_1 = 1.1$ ms and $\tau_2 = 33.0$ ms. Similar to valinomycin, I_{UV}/I_{blue} calculates to 7.5 ± 2.8 (mean±SD). As with valinomycin, a small increase in I ($I_{UV}/I_{blue} = 1.22 \pm 0.01$) was also observed upon UV light illumination in the absence of OptoDArG (Figure S5b); conceivably, this small increment in I may also be partially attributed to heating of the membrane. This is supported by the absorption spectrum of CCCP (Figure S6) that shows a maximum in absorbance between 350 and 400 nm. Critically, in the presence of OptoDArG, blue light exposure at $t = 200$ ms quickly abrogates the UV light-induced current increment

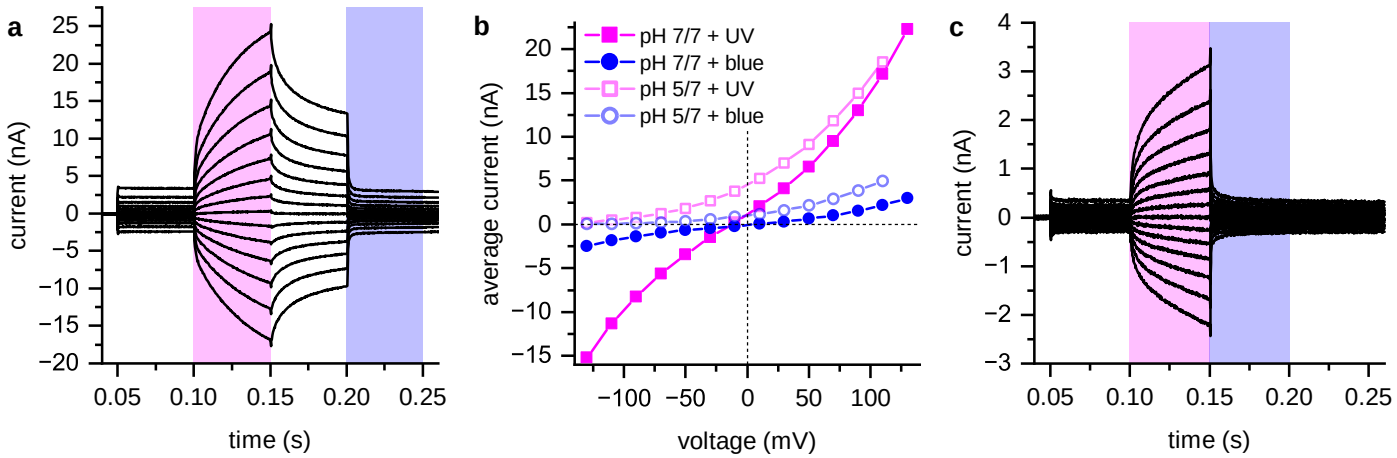

Figure 4: a, Voltage-clamp current recordings on a 70 µm-diameter photoswitchable PLB (*E. coli* PLE + 20 m% OptoDArG) with 10 µM CCCP added to the aqueous compartments (100 mM KCl, 20 mM HEPES pH 7.0) on both sides. Recordings were made as in Figure 2a. **b,** I/V curves constructed as described in Figure 2b for recordings under symmetric ($c'_{H^+} = c''_{H^+} = 1 \times 10^{-7}$ M) and asymmetric ($pH_1 = 5$, $pH_2 = 7$) conditions. **c,** 85 µm-diameter photoswitchable PLB with 2.5 µM CCCP added to the aqueous compartments (15 mM KCl, 10 mM HEPES pH 7.4) on both sides. Voltage protocol as in panel **a**. In contrast to panel **a**, UV light exposure between 100 and 150 ms was immediately followed by blue light from 150 to 200 ms.

(Figure 4a). Taken together, photolipid photoisomerization is primarily responsible for rapid modulation of CCCP currents, as observed for the cationic K^+ ionophore valinomycin.

That said, the current kinetics of CCCP (Figure 4a) and valinomycin (Figure 2a) are distinct. This distinction likely arises from differential effects of OptoDArG photoisomerization on the local partitioning of charged and neutral molecules. As discussed above, this mechanism is exemplified by the 24-fold [BFL77] versus 7-fold [BFL77; Nag+08] permeability increases of the positively charged valinomycin–K^+ complex versus the free carrier and water molecules.

An explanation that first comes into mind is the influence of the membrane dipole potential, Φ_d, which repels positively charged ions, like the valinomycin–K^+ complex [Poh+98]. Φ_d itself may be modulated by OptoDArG photoisomerization considering that (i) Φ_d depends on lipid packing, specifically the number of lipid dipoles per unit surface area and oriented water molecules at the membrane surface [Poh+00] and (ii) azobenzene has a dipole moment of 0 D in its trans state but 3 D in its cis state [HL39] (Figure 1e). If a reduction in Φ_d was decisive, we would have expected opposite effects for positively and negatively charged permeating species [Poh+98]; namely, an increase in the valinomycin–K^+ current and a decrease in CCCP conductance. Consequently, photoinduced changes in Φ_d can be ruled out as primary drivers of the observed conductivity changes.

A second hypothesis would be a decreased hydrophobicity of the membrane interior. Therefore, we have to assume that the thinned cis state bilayers are structurally comparable to highly unsaturated membranes. Consequently, they have an increased water content as can be inferred from the increased water permeability [Olb+00]. The increased hydrophilicity would favor the local partitioning of charged molecules, e.g., the CCCP anion from the bulk. Indeed, the relatively slow increase in I with CCCP and UV light (Figure 4a) may be rationalized by a gradual increase in intramembrane CCCP concentration. Switching to the trans bilayer state with blue light forces both water and CCCP anions out of the membrane, resulting in an instant drop of I. Significantly, this mechanism does not contradict the previously proposed explanation for the rapid increase in valinomycin current (see subsubsection 2.1.1). Since valinomycin is so much more hydrophobic than CCCP, its

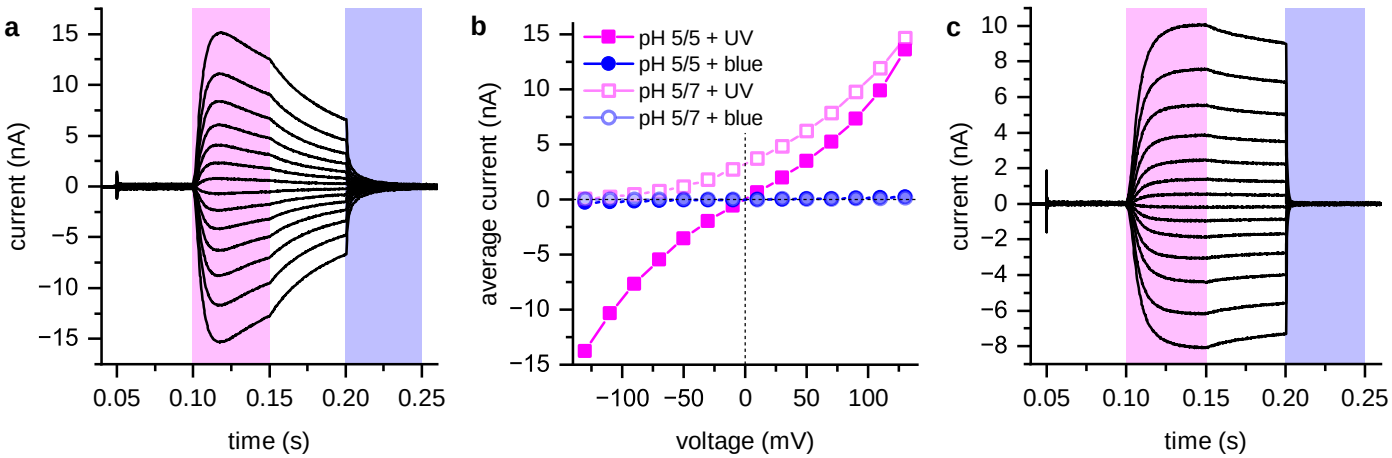

Figure 5: a, Voltage-clamp current recordings on a 70 µm-diameter photoswitchable PLB folded from a lipid mixture containing 79 m% *E. coli* PLE + 20 m% OptoDArG + 1 m% NB-lipid bathed in 100 mM KCl, 20 mM MES pH 5.0. Recordings were made as in Figure 2a. **b,** I/V curves were constructed as described in Figure 2b whereby symmetric conditions were $pH_1 = pH_2 = 5$ and asymmetric conditions $pH_1 = 5$ and $pH_2 = 7$. **c,** PLB prepared as in panel **a** but in a solution containing 15 mM KCl, 10 mM HEPES pH 7.4. Recordings were made as in panel **a**.

concentration in the membrane core cannot readily increase due to a flux from the aqueous bulk.

Importantly, we can rule out temperature and photodynamic effects since the large increase in CCCP current with UV light is (i) absent without photolipid (Figure S5b) and (ii) abrogated effectively upon blue light illumination ($t = 200$ ms in Figure 4a). The ability to rapidly modulate membrane conductance is emphasized in Figure 4c in which the blue laser is triggered immediately after the UV laser is turned-off, resulting in immediate abrogation of I_{UV}.

2.3 NB-lipid facilitates UV light-activated proton-selective currents in photoswitchable bilayers

Considering the application of photolipid-based ion transport regulation in the biological system or the synthetic cell, low background activity in combination with effective on–off modulation may be key. To that effect, we made use of the cationic dye nile blue (NB), a positively-charged benzophenoxazine-based red fluorescent dye that shows pronounced solvatochromism [JB06]. It has previously been described as an uncoupler of intact mitochondria [MA83]. This observation suggests that NB can act as a protonophore. With a pK_a around 10, NB is predominantly protonated, thus cationic, in water at neutral pH [Mad+13]. Since then, lipidated derivatives of other protonatable fluorophores were indeed described to act as cationic protonophores, e.g., rhodamine 19 dodecyl ester (C_{12}R1) and 10-(6'-plastoquinonyl) decylrhodamine 19 (SkQR1) [Ant+11; Rok+13] were described to act as cationic protonophores. We now employed a lipidated analogue of NB which we termed **NB-lipid** (structure in Figure 1d), using an undecyl sidechain as a lipid anchor (this may lower the pK_a somewhat [Pas+18] but the protonated monocationic AH^+ form which is stabilized by resonance should still be dominant in water at neutral pH).

Measurements on PLBs folded from lipid mixtures containing 20 m% OptoDArG and 1 m% NB-lipid demonstrated impressive UV light-activated currents (Figure 5ac). NB-lipid also incorporated into PLBs when added into the aqueous phase (e.g., Figure 7). In a 100-fold $[H^+]$ gradient ($\Delta pH = 2$), V_r of the UV-evoked currents was large and negative (Figure 5b, experimental $V_r = -138$ mV, close to the anticipated -118 mV). Considering that NB-lipid can exist in a deprotonated neutral and protonated cationic form, this result indicates that NB-lipid transports H^+ (see discussion on cationic protonophores below). This transport is selective:

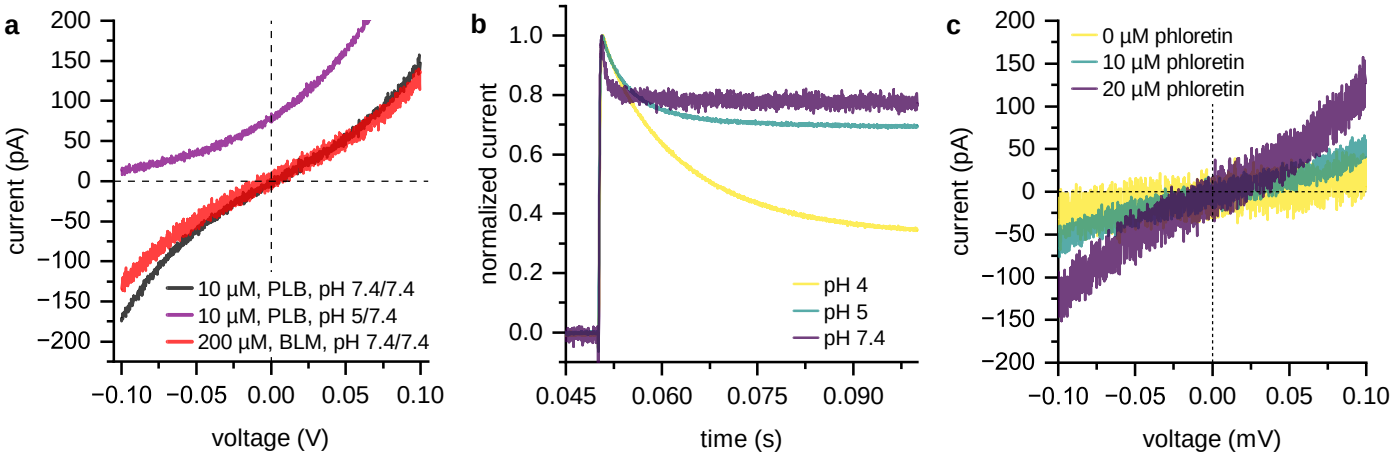

Figure 6: a, Voltage-clamp current recordings on a 135 µm-diameter PLB (black and purple trace) and a 200 µm-diameter black lipid membrane (BLM, red trace) in the presence of 10 µM and 200 µM $[\text{NB-lipid}]_{\text{aq}}$, respectively, added from a 5 mM stock in DMSO to both compartments. Lipid was *E. coli* PLE + 20 m% OptoDArG. The lipid mixtures were not exposed to UV light and hence OptoDArG was present in its trans state. The BLM was painted from 20 mg mL^{-1} lipid in *n*-decane. Buffer was symmetric 15 mM KCl, 10 mM HEPES pH 7.4 (black and red trace); pH in compartment 1 was made 5 by the addition of HCl (purple trace). Both compartments were stirred by magnetic PTFE-coated stir bars. Voltage ramps were recorded after >50 min incubation in the presence of $[\text{NB-lipid}]_{\text{aq}}$: 0.5 s at −100 mV, increase to 100 mV at 100 mV s^{-1}, 0.5 s at 100 mV; the constant-voltage segments are not shown. **b,** Voltage-clamp current recordings on 75 µm-diameter photoswitchable PLBs folded from *E. coli* PLE + 20 m% OptoDArG with OptoDArG in its trans state. NB-lipid was added to the aqueous phase. $V = 130$ mV at $t = 50$ ms, 0 mV before. Buffer solutions were 100 mM KCl, 20 mM MES pH 5, 20 µM phloretin (yellow trace), pH 4 by symmetric addition of 9% HCl (green trace), and 15 mM KCl, 10 mM HEPES pH 7.4, no phloretin (purple trace, separate experiment). For comparison, I was normalized. **c,** PLB folded from *E. coli* PLE + 1 m% NB-lipid in 15 mM KCl, 10 mM HEPES pH 7.4. Phloretin was added from a 1 M stock in ethanol to a final concentration of 10 µM and 20 µM. Voltage ramp recordings as in panel **a**.

Upon creating a 150 mM to 15 mM KCl gradient at symmetrical pH, neither did the increase in [KCl] increase conductance, nor did V_{r} shift considerably from 0 mV (Figure S7).

As with valinomycin and CCCP, blue light abrogated the current increment, again demonstrating excellent reversibility owing to photolipid photoisomerization. Critically, NB-lipid could be modulated very effectively by light exposure: $I_{\text{UV}}/I_{\text{blue}}$ calculates to 60 ± 19 in Figure 5a. In contrast, in the absence of OptoDArG, 1 m% NB-lipid does neither appreciably increase basal membrane conductance nor membrane conductance upon UV light exposure (Figure S5c). As before, these observations point to photolipid-based alterations in bilayer structure as the key modulator.

In contrast to valinomycin and CCCP, I peaks and subsequently decreases during constant UV light exposure in Figure 5a. We reasoned that this may be due to diffusion polarization. As described in Section S4, we tested this hypothesis by conducting experiments at pH 5 and increasing buffer capacity, $\mathfrak{B}$. The resulting current recordings do not differ significantly from each other. Hence, diffusion polarization is not the reason for the peculiar shape of the current traces recorded at pH 5. However, we did observe an effect of pH on current kinetics. Current traces recorded in HEPES buffer at pH 7.4 ($\mathfrak{B} = 5.7$ mM; $\text{p}K_{\text{a}} = 7.48$ at 25°C [Goo+66]) are shown in Figure 5c: Clearly, the decrease in I during UV light illumination is absent and $I_{\text{UV}}/I_{\text{blue}}$ calculates to 229 ± 27. This observation led us to consider that the effect of pH on NB-lipid current kinetics may originate from a cationic protonophore transport mechanism which involves current relaxations at low pH [Rok+13].

2.3.1 NB-lipid: cubic currents, current relaxation and sensitivity to phloretin point towards a cationic ionophore transport mechanism

Here, we demonstrate that NB-lipid functions as a cationic protonophore involving its A and AH^+ form. In these experiments [Rok+13], we frequently measure basal NB-lipid currents in the presence of trans-OptoDArG which are denoted by I_b.

At low pH, I_b relaxes following voltage application. NB-lipid current kinetics depend on bulk pH, as shown in Figure 5ac. At pH 5, I peaked and subsequently relaxed during UV light exposure (Figure 5a and Figure S3). In contrast, no such relaxation was observed at pH 7.4 (Figure 5c and Figure S8a). This relaxation is characteristic of ionophore currents, where changes in the transport rates caused by voltage application influence the system. For cationic protonophores, current relaxations are amplified at lower pH. This is because effective H^+ transport by cationic protonophores requires fast interleaflet movement and adequate supply of uncharged carriers which becomes depleted at low pH [Rok+13; BM83; KBM84; OH83]. Then, voltage-induced changes in k_a can lead to a gradient of charged species within the membrane, reducing the H^+ transport capacity. The resulting decay in current reflects intramembrane protonophore rearrangement. Protonation and deprotonation reactions at the interface (k_A and k_D) occur much faster than bulk transport. The relaxation in I can be quantified by two parameters: the relaxation time constant (τ) and the fractional decrease in current $\alpha_r = I_0/I_\infty - 1$ [Rok+13]. Indeed, as shown in Figure 6b, we tentatively observe a successive increase in both τ and α_r as pH is decreased from 7.4 to 5 to 4 in NB-lipid-containing photoswitchable PLBs. NB-lipid exhibits higher rates of current relaxation, $1/\tau$, than $C_{12}R1$ and SkQR1 [Rok+13]. This may be due to higher transport rates and/or a difference in pK_a (cf. Equation 11 in [Rok+13]). The observed relaxation is strong evidence supporting a cationic protonophore transport mechanism for NB-lipid.

I_b/V is cubic (non-ohmic). Transmembrane transport of a membrane-adsorbed charged carrier is alike that of a hydrophobic ion and thus depends on membrane electrostatic potentials [Hla72; HHP19]. These are, in particular, the transmembrane potential, V, and Φ_d. The latter evokes supralinearity of the I/V curve. Taylor expansion of the exact relation results in a cubic dependence of I on V [HHP19]:

$$I(V) = g_0 \cdot (1 + \alpha_v V^2) \cdot V + o \tag{5}$$

where $I(V)$ is current at a particular voltage, g_0 conductance at $V = 0$ and α_v is a supralinearity factor [Han17]; o accounts for a small current offset. We measured cubic I/V curves for NB-lipid (Figure 4b) which were enlarged by UV light (Figure 5b and Figure S7c). CCCP (Figure 4b) [KBM84] and the cationic protonophore SkQR1 [Rok+13] exhibit cubic I/V relationships, suggesting a similar carrier-based transport mechanism for NB-lipid. In contrast, a channel mechanism of transport can be ruled out because for this case the Goldman–Hodgkin–Katz flux equation predicts a linear (ohmic) I/V relationship at symmetric c_{H^+} [Hil01].

A reduction in Φ_d by phloretin increases currents. Introduced above, Φ_d is a membrane intrinsic positive electrostatic potential that favors anion but opposes cation permeation [FH86; HHP19]. The natural phenol phloretin adsorbs to lipid bilayers and thereby reduces Φ_d [Poh+97]. This reduction in Φ_d reduces the flux of $CCCP^-$ and hence I, but increases the flux of $C_{12}R1$ and SkQR1 because those permeate the membrane as cations [Rok+13]. Hence, if NB-lipid was a cationic protonophore, I should be amplified by the addition of phloretin. Indeed, this is what we observed: The symmetric addition of 10 µM and 20 µM phloretin to a PLB (*E. coli* PLE + 1 m% NB-lipid) successively increased conductance (Figure 6c). As expected, the effect on

CCCP currents was opposite. Again, the observation that a reduction in Φ_d coincides with an increase in I qualitatively agrees with a cationic protonophore mechanism for NB-lipid.

2.3.2 NB-lipid currents are sensitive to membrane thickness and its modulation

In our experiments with NB-lipid, large on–off current modulations were reliably observed (Figure S8a). Two observations may explain the apparent variation in NB-lipid currents: (i) d_m in the presence of trans-OptoDArG can vary, as suggested by specific bilayer capacitance variations, potentially due to residual solvent between leaflets or PLB compositional differences. (ii) The light-evoked capacitance change – and hence the change in d_m – also varied (Figure S8b). Pronounced sensitivity to d_m likely explains the effective on–off regulation of NB-lipid currents by modest d_m changes upon photoisomerization (UV light-induced cis-OptoDArG thins the membrane; see Figure 1c).

To demonstrate the strong dependence of NB-lipid-mediated currents on membrane thickness (d_m), we compared solvent-depleted PLBs (folded from monolayers) and decane-containing black lipid membranes (BLMs are "painted" from lipid in *n*-decane [HP18] and solvent retained between the leaflets renders them thicker, lowering their specific capacitance), both prepared from the same lipid mixture (*E. coli* PLE + 20 m% OptoDArG). We incubated both PLBs and BLMs under continuous stirring for >50 min with NB-lipid added in various concentrations $[\text{NB-lipid}]_{aq}$ to the aqueous compartments (Figure S10 shows the time course of conductance increase for the PLB). Voltage ramps revealed that both a BLM with 200 µM $[\text{NB-lipid}]_{aq}$ (red trace in Figure 6a) and a PLB with 10 µM $[\text{NB-lipid}]_{aq}$ (black trace in Figure 6a) reached $g_0 \approx 1$ nS, despite the BLM having twice the area. This emphasizes a strong dependence of NB-lipid currents on d_m.

Albeit NB-lipid current regulation by photolipid-mediated bilayer structural changes aligns with our findings with valinomycin and CCCP, we also explored other mechanisms by which UV light could have increased NB-lipid currents. As detailed in Section S5, we can exclude significant contributions from photodynamic bilayer modifications or membrane temperature at typical NB-lipid concentrations (e.g., Figure 5). Temperature-related effects require higher NB-lipid concentrations (see below).

2.3.3 Membrane heating at excess NB-lipid concentrations evokes impressive currents

Unlike valinomycin and CCCP, NB is a well-established chromophore that effectively absorbs light with high extinction coefficient [JB06]. Despite significant fluorescence quantum yields in water or lipid media, most of the energy it absorbs is converted into heat through molecular vibrations. Heat generated by photothermal absorbers at the membrane can cause an increase in membrane temperature [Ras+20], leading to membrane area expansion, thickness reduction [KNK11], and increased capacitance (cf. Equation 1). The photothermal optocapacitive approach builds on these effects [Sha+12; Ras+20; Car+18]. Photothermal heating may also increase NB-lipid currents, yet, with kinetics distinct from those induced by photolipid photoisomerization. Considering the thermal rate of capacitance increase of $\approx$0.3 % °C^{-1} [Pla+18], increments in capacitance comparable to those observed upon photoisomerization ($\approx$12%, see Figure S8b) may not be readily achievable.

Indeed, at high NB-lipid concentrations in PLBs without OptoDArG, both UV and blue light exposure cause an increase in I, as can be seen in Figure 7ab. This is attributed to changes in membrane properties resulting from a photothermal increase in temperature. However, in sharp contrast to Figure 5ac, the UV light-evoked I decays fully immediately after turning-off the laser. This spontaneous reduction in I emphasizes the transient

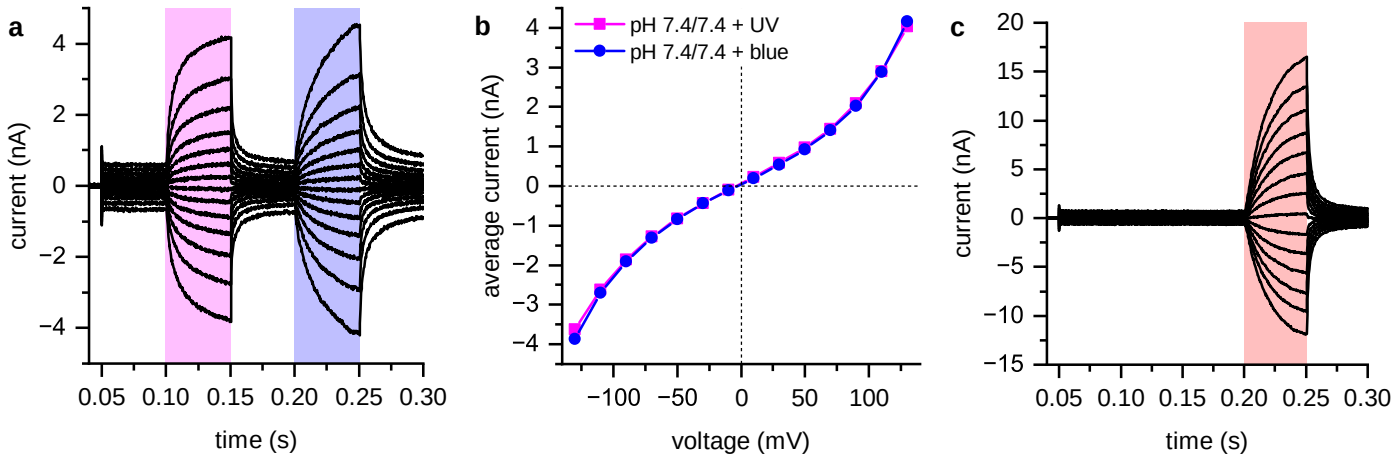

Figure 7: a, Voltage-clamp current recordings on a PLB folded from *E. coli* PLE (without photolipid and NB-lipid added to the lipid mixture) bathed in 15 mM KCl, 10 mM HEPES pH 7.4. NB-lipid was added to the aqueous compartments at a concentration of 25 µM from a 1 mM stock in DMSO. Voltage and light application as in Figure 2a. **b,** I/V curves constructed from the current traces in panel **a**. As before, I_{blue} was calculated by averaging I between 225 and 250 ms (blue circles); I_{UV} by averaging I between 125 and 150 ms (magenta squares). **c,** Same PLB and voltage application as in panel **a**. Between 200 and 250 ms the PLB was exposed to intense red (640 nm) light, close to the excitation maximum of nile blue.

nature of membrane heating which reverts spontaneously due to heat dissipation; this is in sharp contrast to increases in I upon UV light exposure in photoswitchable bilayers that persist even as the UV laser is turned-off – a consequence of the presence of distinct photoisomers (emphasized in Figure S9b). In addition, at excess NB-lipid concentrations, blue light also causes an increase in I which decays immediately upon turning-off the laser (Figure 7a). Exposure of the same PLB as in Figure 7a to intense red laser light (640 nm, close to the absorption maximum of NB at 639 nm [Bau+23]), evokes several-fold larger currents with an identical temporal behavior (Figure 7c). Taken together, these results evidence that light-evoked changes in membrane temperature contribute to the currents observed in Figure 5 but are negligible in comparison to the effects deriving from alterations in bilayer material properties due to photolipid photoisomerization. To the best of our knowledge, this is the first study in which rapid changes in membrane temperature were used to regulate carrier currents.

3 Discussion

H^+ transport across lipid bilayers, facilitated by a novel lipidated nile blue derivative, NB-lipid, is very effectively modulated by photolipids. At neutral pH, the generated photo-currents are comparable in magnitude (Figure 5c, Figure S8) to those elicited by the human proton channel H_V1 or channelrhodopsins (ChR) in transfected cells [Boy+23; Nag+02]. As in the case of H_V1 or ChR2, the current is highly selective for protons. Yet, the proton-to-sodium permeability ratio P_{H^+}/P_{Na^+} for ChR2 was only 2×10^6 to 6×10^6, resulting at neutral pH in a dominant Na^+ component in mammalian brains [DH17]. In contrast, even in a high-salt environment and at pH 7.4, the contribution of the salt to the reversal potential of a NB-lipid-containing cis state membrane was negligible (Figure S7). Hence, we conclude that NB-lipid is highly proton-selective (Figure 5), even in high-salt conditions.

Photolipids and NB-lipid can be administered directly into the aqueous solution (ref. [Bas+24] and Figure 6), offering immediate availability for rapid intervention. However, this photopharmacological aspect of our approach may result in less precise delivery, as both compounds can be absorbed by off-target cells. This limitation can be partly mitigated by precise illumination and the fact that transient increases in proton permeability in

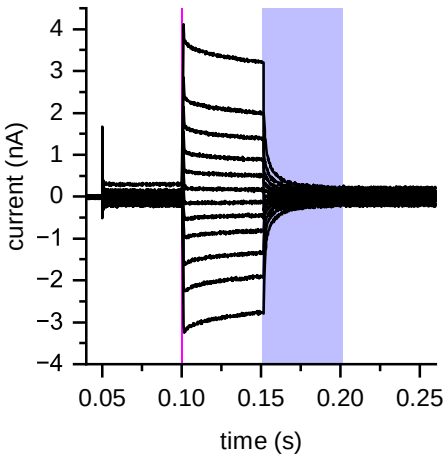

Figure 8: Voltage-clamp current recordings on a 85 µm-diameter photoswitchable PLB folded from 79 m% *E. coli* PLE + 20 m% OptoDArG + 1 m% NB-lipid in 15 mM KCl, 10 mM HEPES pH 7.4. The PLB was exposed to UV light for 1 ms at $t = 100$ ms and to blue light for 50 ms at $t = 151$ ms. Voltage application as in Figure 2a whereby V ranged from 110 mV to −110 mV.

non-excitable cells may not cause noticeable effects. Overall, the optogenetic approach, which targets specific cell types via genetic transfection, and the photopharmacological approach here introduced to selectively modulate H^+ permeability, appear to be complementary strategies.

A feature important for future NB-lipid applications is its exceptionally low background permeability. We observed a nearly 200-fold photoinduced augmentation of the proton current. This unusually high amplification of proton currents likely arises because the permeating species is a cation [HHP19]. The most effective protonophores are based on anion transport for a reason: The hydrophobic membrane interior harbors a positive dipole potential, Φ_d, repelling cations and attracting anions. In other words, Φ_d lowers the energy barrier for anionic protonophores (e.g., CCCP), while raising it for cationic ones (e.g., NB-lipid) [HHP19]. This explains the exceptionally low membrane permeability of NB-lipid in the dark. On a qualitative level, the photolipid effect is independent of charge, i.e., UV illumination increases proton permeability for both NB-lipid and CCCP, supporting the idea that changes in bilayer material properties underlie the effect.

We found that photolipid-mediated changes in bilayer thickness play a crucial role in the effective photomodulation of selective H^+ currents with NB-lipid. Atomic force microscopy experiments on membranes harboring photoswitchable ceramides revealed light-induced bilayer thickness changes exceeding 1.5 nm [Fra+16a]. Notably, these ceramides had only one azobenzene moiety per acyl chain. In our experiments, we employ photolipids where both acyl chains contain azobenzene moieties. This should lead to larger thickness changes, potentially locally reducing bilayer thickness to just ≈1–2 nm at sites where OptoDArG molecules from the opposing leaflets align. At such sites, the resulting electric field would be highly focused, with enormous field strengths facilitating the flip of the cationic NB-lipid across the bilayer. This conclusion is in line with previously observed large-amplitude potential fluctuations in lipid bilayers [Tar+18]. These are also essential for the proton background permeability in the absence of protonophores [Lee+24]. Photolipids are likely to amplify these fluctuations of the electric field strength since they only constitute a minor membrane fraction and thus introduce thickness inhomogeneities when switched to their cis state.

The comparison between cationic and anionic protonophores highlights the potential to optimize ionophore structure for achieving selective, effectively on–off modulated carrier currents in photoswitchable membranes. Notably, the photoisomerization of photolipid-doped lipid bilayers may gate not only proton-selective carrier

currents, but be extended to K^+, Na^+, or Ca^{++}-selective currents, eventually even anion translocation. As with proton-selective currents, there is little doubt that the regulation of these currents can be reversible and, depending on irradiance, rapid. To that effect, we have already shown here that K^+-selective currents across photoswitchable bilayers carried by valinomycin are amplified upon UV light exposure and rapidly turned-off upon blue light exposure. The reversibility of photomodulation demonstrates that neither in the case of photoinduced H^+ nor K^+ currents, changes in membrane temperature were determining. Likewise, we provided evidence that photodynamic membrane damage was not involved at the assayed timescales.

Whilst we used 50 ms light pulses for photoisomerization in this study to assay the kinetics of current build-up and decay, we note that shorter pulses – i.e., less delivered energy – may suffice at modulating carrier activity. This is because the underlying mechanism is photolipid photoisomerization whose rate is proportional to irradiance. This is demonstrated in Figure 8 in which we achieved large on–off regulation of NB-lipid H^+ currents by a 1 ms pulse of UV light.

Hence, we conclude that membrane mechanical alterations evoked by photolipid photoisomerization gate carrier currents. In contrast to specially-developed photoregulated-ion-binding ionophores, or to protein-based optogenetic approaches, the photolipid-based approach allows regulation of well-established carriers that have been in use for decades. We imagine photolipid-regulated carriers as a complementary and convenient all-chemical approach towards achieving light-based ion permeability regulation in the biological and synthetic cell or the artificial neuron, that can valuably distinguish itself from photoregulated-ion-binding ionophores as well as from protein-based optogenetic approaches by, e.g., its large currents, sub-millisecond photoresponse with long-lasting effect, easily tuned ion scope, and the potential to rationally shift its single photon action spectra from the UV/Vis right up to the NIR/SWIR [Bau+23; Bau+24].

4 Material and Methods

4.1 Materials for planar lipid bilayer experiments

E. coli Polar Lipid Extract (PLE, item no. 100600) and 1,2-diphytanoyl-*sn*-glycero-3-phosphocholine (DPhPC, item no. 850356) were obtained from Avanti Polar Lipids (distributed by Merck) and kept at −80 °C. OptoDArG was synthesized by the group of Dr. Glasnov as described previously [Lic+18]. Lipid aliquots and mixtures were prepared within amber glass micro reaction vials from lipids dissolved in chloroform. Prior to storage at −80 °C, solvent was evaporated by a mild vacuum gradient (Rotavapor, Büchi Labortechnik AG) and the dried lipids were flooded with argon. All aqueous buffers used in the PLB experiments were freshly prepared from laboratory-grade dry substances (supplied by VWR, Merck, or Fisher Scientific) dissolved in ultrapure water (>18 MΩ cm, Milli-Q water purification system) and pH-adjusted using a daily-calibrated pH meter (FiveEasy, Mettler Toledo). CCCP (carbonyl cyanide *m*-chlorophenylhydrazone, 98%, Thermo Scientific) and valinomycin were kept as stocks in DMSO. NB-lipid was synthesized in a parallel study, with synthesis and characterization given there as molecule **S43** [Bau+24]. NB-lipid was kept in a dried state at −80 °C and aliquots were prepared in DMSO prior to measurement.

4.2 Horizontal planar lipid bilayer experiments

Planar lipid bilayer (PLB) experiments with laser irradiation for rapid photoisomerization were conducted as described recently [Bas+24]. Solvent-depleted horizontal PLBs were folded from lipids spread on top of aqueous buffer in the lower and upper compartment of a custom-built chamber assembly made from PTFE [MM72; Sai+20]. First, an aperture of around 70 µm in diameter in 25 µm-thick PTFE foil (Goodfellow GmbH) was created by high-voltage discharge – this prepares the septum separating the macroscopic compartments. The PLB diameters given in the main text refer to the size of this aperture. After the septum was treated with 0.6 vol% hexadecane in hexane, hexane was allowed to evaporate for >1 h. The residual hexadecane facilitates the solvent annulus or torus that later laterally anchors the PLB within the aperture [Whi+76]. The septum was attached by silicon paste to the lower side of the upper compartment of the chamber assembly. Lipids at the air–water interfaces were prepared by applying lipid mixtures dissolved in hexane at a concentration of 10 $\mathrm{mg\,mL^{-1}}$ onto both aqueous interfaces. After hexane evaporated, horizontal PLBs were folded by rotation of the upper compartment of the chamber assembly.

A 30 mm-diameter cover glass (No. 1, Assistent, Hecht Glaswarenfabrik GmbH & Co KG) fixed with a threaded PTFE ring comprised the bottom of the lower compartment. The chamber assembly was installed on the sample stage of an Olympus IX83 inverted microscope equipped with an iXon 897 E EMCCD (Andor, Oxford Instruments Group). The chamber holder was equipped with screws for fine translation of the upper compartment in z-direction to position the horizontal PLB within working distance of a 40×/1.30 NA infinity-corrected plan fluorite oil immersion objective (UPLFLN40XO, Olympus) or a 40×/0.65 NA infinity-corrected plan achromat air objective (PLN40X, Olympus). The motorized microscope and real-time controller (U-RTC, Olympus) used for synchronizing lasers and electrophysiological acquisition were controlled using the proprietary cellSens software (Olympus).

For electrical measurements, a Ag/AgCl agar salt bridge containing 0.5 M KCl was put into each compartments and connected to the headstage of an EPC 9 patch-clamp amplifier (HEKA Elektronik, Harvard Bioscience). Headstage and chamber assembly were housed in a Faraday cage. Voltage-clamp measurements were conducted

using PATCHMASTER 2x91 software (HEKA Elektronik, Harvard Biosciences). Current was analogously filtered at 10 kHz by a combination of Bessel filters and acquired at 50 kHz. Data recorded with PATCHMASTER was exported, analyzed and graphed using Mathematica 14 (Wolfram Research) and OriginPro 2024 (OriginLab Corporation).

Rapid photoisomerization of photolipids embedded in horizontal PLBs was achieved by exposure to blue (488 nm diode laser, iBEAM-SMART-488-S-HP, TOPTICA Photonics) and UV laser light (375 nm diode laser, iBEAM-SMART-375-S, TOPTICA Photonics). Both lasers were digitally modulated and separately focused into the back-focal plane of the objective via the ZET488/640rpc main dichroic mirror (Chroma). The diameter of the blue laser profile at the sample stage was ≈58 µm ($1/e^2$) whilst the UV laser profile spanned roughly 150–200 µm (its shape was less defined owing to the absence of a spatial filter). At a software-set output power of 200 mW (blue) and 70 mW (UV), ≈20–30 mW (blue and UV) exited the microscope objective depending on current alignment, as determined by a photodiode (S120VC, Thorlabs).

To achieve intense excitation of membrane-embedded NB-lipid, a red laser (640 nm, iBEAM-SMART-640-S, TOPTICA Photonics) was used. It was operated at 150 mW of which ≈30 mW reached the sample stage. The diameter of the red laser profile at the sample stage was ≈74 µm ($1/e^2$).

4.3 Vertical planar lipid bilayer and black lipid membrane experiments

Vertical PLBs were folded in a similar manner to the description above and as given in [Pfe+21]. The Faraday cage was equipped with a magnetic stirrer positioned underneath the PTFE chamber which allowed for the aqueous compartments on both sides of the vertical PLB to be stirred by magnetic PTFE-coated stir bars. Ag/AgCl agar salt bridges were used. Recordings were made using an EPC 10 patch-clamp amplifier (HEKA Elektronik, Harvard Bioscience).

The same vertical chamber assembly in combination with a PTFE septum containing a larger 200 µm aperture was also used for painting black lipid membranes (BLMs) [HP18]. Therefore, 20 $\mathrm{mg\,mL^{-1}}$ lipid in *n*-decane was used to pretreat the aperture. After drying for around 20 min, the chamber was assembled, buffer was added to both compartments and the lipid solution was spread across the aperture, eventually resulting in a BLM with specific capacitance >0.35 $\mathrm{\mu F\,cm^{-2}}$.

Acknowledgements

This research was funded in whole by the Austrian Science Fund (FWF) grants P36399 and P34826 to Peter Pohl.

References

[Ale+23] Mina Aleksanyan *et al.* Photomanipulation of Minimal Synthetic Cells: Area Increase, Softening, and Interleaflet Coupling of Membrane Models Doped with Azobenzene-Lipid Photoswitches. *Advanced science (Weinheim, Baden-Wurttemberg, Germany).* **10**, e2304336 (2023).

[Ant+11] Yuri N. Antonenko *et al.* Derivatives of rhodamine 19 as mild mitochondria-targeted cationic uncouplers. *The Journal of biological chemistry.* **286**, 17831–17840 (2011).

[Ary+20] Pooja Arya *et al.* Kinetics of photo-isomerization of azobenzene containing surfactants. *Journal of Chemical Physics.* **152**, 024904 (2020).

[Bas+24] Carlos A. Z. Bassetto *et al.* Photolipid excitation triggers depolarizing optocapacitive currents and action potentials. *Nature Communications.* **15**, 1139 (2024).

[Bau+23] Benedikt Baumgartner *et al.* Azobenzenes can achieve near-infrared photocontrol in biological systems, with quantitative Z→E photoisomerization, via singlet manifold photoredox (2023).

[Bau+24] Benedikt Baumgartner *et al.* A general method for near-infrared photoswitching in biology, demonstrated by the >700 nm photocontrol of GPCR activity in brain slices. *ChemRxiv : the preprint server for chemistry* (2024).

[Ben+73] R. Benz *et al.* Valinomycin-mediated ion transport through neutral lipid membranes: influence of hydrocarbon chain length and temperature. *The Journal of Membrane Biology.* **14**, 339–364 (1973).

[BFL77] R. Benz, O. Fröhlich, and P. Läuger. Influence of membrane structure on the kinetics of carrier-mediated ion transport through lipid bilayers. *Biochimica Et Biophysica Acta.* **464**, 465–481 (1977).

[BM83] R. Benz and S. McLaughlin. The molecular mechanism of action of the proton ionophore FCCP (carbonylcyanide p-trifluoromethoxyphenylhydrazone). *Biophysical Journal.* **41**, 381–398 (1983).

[Boy+05] Edward S. Boyden *et al.* Millisecond-timescale, genetically targeted optical control of neural activity. *Nature neuroscience.* **8**, 1263–1268 (2005).

[Boy+23] Danila Boytsov *et al.* Trapped Pore Waters in the Open Proton Channel HV 1. *Small (Weinheim an der Bergstrasse, Germany).* **19**, e2205968 (2023).

[BS55] Hans Brockmann and Günter Schmidt–Kastner. Valinomycin I, XXVII. Mitteil. über Antibiotica aus Actinomyceten. *Chemische Berichte.* **88**, 57–61 (1955).

[Car+15] João L. Carvalho-de-Souza *et al.* Photosensitivity of neurons enabled by cell-targeted gold nanoparticles. *Neuron.* **86**, 207–217 (2015).

[Car+18] João L. Carvalho-de-Souza *et al.* Optocapacitive Generation of Action Potentials by Microsecond Laser Pulses of Nanojoule Energy. *Biophys J.* **114**, 283–288 (2018).

[Cre+22] Fucsia Crea *et al.* Photoactivation of a Mechanosensitive Channel. *Frontiers in molecular biosciences.* **9**, 905306 (2022).

[Dei11] Karl Deisseroth. Optogenetics. *Nature Methods.* **8**, 26–29 (2011).

[DH17] Karl Deisseroth and Peter Hegemann. The form and function of channelrhodopsin. *Science (New York, N.Y.)* **357** (2017).

[Ern+14] Oliver P. Ernst *et al.* Microbial and animal rhodopsins: structures, functions, and molecular mechanisms. *Chemical reviews.* **114**, 126–163 (2014).

[FH86] R. F. Flewelling and W. L. Hubbell. The membrane dipole potential in a total membrane potential model. Applications to hydrophobic ion interactions with membranes. *Biophysical Journal.* **49**, 541–552 (1986).

[Fir+23] Alexander M. Firsov *et al.* Photodynamic activity rather than drilling causes membrane damage by a light-powered molecular nanomotor. *Journal of photochemistry and photobiology. B, Biology.* **239**, 112633 (2023).

[Fra+16a] James Allen Frank *et al.* Optical Control of Lipid Rafts with Photoswitchable Ceramides. *J Am Chem Soc.* **138**, 12981–12986 (2016).

[Fra+16b] James Allen Frank *et al.* Photoswitchable diacylglycerols enable optical control of protein kinase C. *Nature chemical biology.* **12**, 755–762 (2016).

[Gar+17] Víctor García-López *et al.* Molecular machines open cell membranes. *Nature.* **548**, 567–572 (2017).

[Goo+66] N. E. Good *et al.* Hydrogen ion buffers for biological research. *Biochemistry.* **5**, 467–477 (1966).

[Han17] Christof Hannesschlaeger. "Transmembrane Diffusion of Poorly Partitioning or Self Inhibiting Solutes". Doctoral Thesis. Johannes Kepler University Linz, 2017.

[HHP19] Christof Hannesschlaeger, Andreas Horner, and Peter Pohl. Intrinsic Membrane Permeability to Small Molecules. *Chem Rev.* **119**, 5922–5953 (2019).

[Hil01] Bertil Hille. *Ion channels of excitable membranes.* 3rd ed. Sunderland, Mass.: Sinauer Associates, 2001.

[HL39] G. S. Hartley and R. J. W. Le Fèvre. 119. The dipole moments of cis- and trans-azobenzenes and of some related compounds. *Journal of the Chemical Society.* **0**, 531–535 (1939).

[Hla72] S. B. Hladky. The steady-state theory of the carrier transport of ions. *The Journal of Membrane Biology.* **10**, 67–91 (1972).

[HLF95] S. B. Hladky, J. C. Leung, and W. J. Fitzgerald. The mechanism of ion conduction by valinomycin: analysis of charge pulse responses. *Biophysical Journal.* **69**, 1758–1772 (1995).

[HMT18] Katharina Hüll, Johannes Morstein, and Dirk Trauner. In Vivo Photopharmacology. *Chem Rev.* **118**, 10710–10747 (2018).

[HN13] Peter Hegemann and Georg Nagel. From channelrhodopsins to optogenetics. *EMBO molecular medicine.* **5**, 173–176 (2013).

[HP18] Christof Hannesschlaeger and Peter Pohl. Membrane Permeabilities of Ascorbic Acid and Ascorbate. *Biomolecules.* **8** (2018).

[HP62] P. G. Heytler and W. W. Prichard. A new class of uncoupling agents–carbonyl cyanide phenylhydrazones. *Biochemical and biophysical research communications.* **7**, 272–275 (1962).

[JB06] Jiney Jose and Kevin Burgess. Benzophenoxazine-based fluorescent dyes for labeling biomolecules. *Tetrahedron.* **62**, 11021–11037 (2006).

[Joh23] T. Johnson. "Molecular machines for controlling transmembrane ion transport". PhD thesis. University of Oxford, 2023.

[KBM84] J. Kasianowicz, R. Benz, and S. McLaughlin. The kinetic mechanism by which CCCP (carbonyl cyanide m-chlorophenylhydrazone) transports protons across membranes. *The Journal of membrane biology.* **82**, 179–190 (1984).

[KES71] S. Krasne, G. Eisenman, and G. Szabo. Freezing and melting of lipid bilayers and the mode of action of nonactin, valinomycin, and gramicidin. *Science (New York, N.Y.)* **174**, 412–415 (1971).

[Kle+11] Sonja Kleinlogel *et al.* A gene-fusion strategy for stoichiometric and co-localized expression of light-gated membrane proteins. *Nature Methods.* **8**, 1083–1088 (2011).

[KNK11] Norbert Kučerka, Mu-Ping Nieh, and John Katsaras. Fluid phase lipid areas and bilayer thicknesses of commonly used phosphatidylcholines as a function of temperature. *Biochim Biophys Acta.* **1808**, 2761–2771 (2011).

[Läu72] P. Läuger. Carrier-mediated ion transport. *Science (New York, N.Y.)* **178**, 24–30 (1972).

[Leb71] O. H. Leblanc. The effect of uncouplers of oxidative phosphorylation on lipid bilayer membranes: Carbonylcyanidem-chlorophenylhydrazone. *The Journal of Membrane Biology.* **4**, 227–251 (1971).

[Lee+24] Seonwoo Lee *et al.* Dynamic Second Harmonic Imaging of Proton Translocation Through Water Needles in Lipid Membranes. *Journal of the American Chemical Society* (2024).

[Lic+18] Michaela Lichtenegger *et al.* An optically controlled probe identifies lipid-gating fenestrations within the TRPC3 channel. *Nat Chem Biol.* **14**, 396–404 (2018).

[MA83] M. S. Mai and W. S. Allison. Inhibition of an oligomycin-sensitive ATPase by cationic dyes, some of which are atypical uncouplers of intact mitochondria. *Archives of biochemistry and biophysics.* **221**, 467–476 (1983).

[Mad+13] Jeppe Madsen *et al.* Nile Blue-based nanosized pH sensors for simultaneous far-red and near-infrared live bioimaging. *Journal of the American Chemical Society.* **135**, 14863–14870 (2013).

[MM22] Venkata Shiva Mandala and Roderick MacKinnon. Voltage-sensor movements in the Eag Kv channel under an applied electric field. *Proceedings of the National Academy of Sciences.* **119**, e2214151119 (2022).

[MM72] M. Montal and P. Mueller. Formation of bimolecular membranes from lipid monolayers and a study of their electrical properties. *Proc Natl Acad Sci U S A.* **69**, 3561–3566 (1972).

[Mül+22] Markus Müller *et al.* BTDAzo: A Photoswitchable TRPC5 Channel Activator. *Angewandte Chemie (International ed. in English).* **61**, e202201565 (2022).

[Mül+24] Markus Müller *et al.* Ideal efficacy photoswitches for TRPC4/5 channels harness high potency for spatiotemporally-resolved control of TRPC function in live tissues. *bioRxiv* (2024).

[Nag+02] Georg Nagel *et al.* Channelrhodopsin-1: a light-gated proton channel in green algae. *Science (New York, N.Y.)* **296**, 2395–2398 (2002).

[Nag+08] John F. Nagle *et al.* Theory of passive permeability through lipid bilayers. *Journal of General Physiology.* **131**, 77–85 (2008).

[Obe+22] Martina F. Ober *et al.* SAXS measurements of azobenzene lipid vesicles reveal buffer-dependent photoswitching and quantitative Z→E isomerisation by X-rays. *Nanophotonics.* **11**, 2361–2368 (2022).

[OH83] K. O'Shaughnessy and S. B. Hladky. Transient currents carried by the uncoupler, carbonyl cyanide m-chlorophenylhydrazone. *Biochimica Et Biophysica Acta.* **724**, 381–387 (1983).

[Olb+00] K. Olbrich *et al.* Water permeability and mechanical strength of polyunsaturated lipid bilayers. *Biophys J.* **79**, 321–327 (2000).

[Pas+18] Alina A. Pashkovskaya *et al.* Mechanism of Long-Chain Free Fatty Acid Protonation at the Membrane-Water Interface. *Biophys J.* **114**, 2142–2151 (2018).

[Per+17] Carla Pernpeintner *et al.* Light-Controlled Membrane Mechanics and Shape Transitions of Photoswitchable Lipid Vesicles. *Langmuir.* **33**, 4083–4089 (2017).

[Pfe+21] Juergen Pfeffermann *et al.* Photoswitching of model ion channels in lipid bilayers. *Journal of photochemistry and photobiology. B, Biology.* **224**, 112320 (2021).

[Phi+09] Rob Phillips *et al.* Emerging roles for lipids in shaping membrane-protein function. *Nature.* **459**, 379–385 (2009).

[Pla+18] Michael Plaksin *et al.* Thermal Transients Excite Neurons through Universal Intramembrane Mechanoelectrical Effects. *Physical review. X.* **8** (2018).

[Poh+00] E. E. Pohl *et al.* Changes of intrinsic membrane potentials induced by flip-flop of long-chain fatty acids. *Biochemistry.* **39**, 1834–1839 (2000).

[Poh+97] P. Pohl *et al.* Permeation of phloretin across bilayer lipid membranes monitored by dipole potential and microelectrode measurements. *Biochimica Et Biophysica Acta.* **1323**, 163–172 (1997).

[Poh+98] E. E. Pohl *et al.* Changes of the membrane potential profile induced by verapamil and propranolol. *Biochimica Et Biophysica Acta.* **1373**, 170–178 (1998).

[Ras+20] Sahil K. Rastogi *et al.* Remote nongenetic optical modulation of neuronal activity using fuzzy graphene. *Proceedings of the National Academy of Sciences.* **117**, 13339–13349 (2020).

[RH74] Mary Callaghan Rose and Robert W. Henkens. Stability of sodium and potassium complexes of valinomycin. *Biochimica et biophysica acta. General subjects.* **372**, 426–435 (1974).

[Rok+13] Tatyana I. Rokitskaya *et al.* Electrogenic proton transport across lipid bilayer membranes mediated by cationic derivatives of rhodamine 19: comparison with anionic protonophores. *European biophysics journal : EBJ.* **42**, 477–485 (2013).

[RT21] Arundhati Roy and Pinaki Talukdar. Recent Advances in Bioactive Artificial Ionophores. *Chembiochem : a European journal of chemical biology.* **22**, 2925–2940 (2021).

[Sai+20] Ali Saitov *et al.* Ordered Lipid Domains Assemble via Concerted Recruitment of Constituents from Both Membrane Leaflets. *Phys Rev Lett.* **124**, 108102 (2020).

[Sha+12] Mikhail G. Shapiro *et al.* Infrared light excites cells by changing their electrical capacitance. *Nature Communications.* **3**, 736 (2012).

[Tar+18] Orly B. Tarun *et al.* Label-free and charge-sensitive dynamic imaging of lipid membrane hydration on millisecond time scales. *Proceedings of the National Academy of Sciences.* **115**, 4081–4086 (2018).

[Urb+18] Patrick Urban *et al.* Light-Controlled Lipid Interaction and Membrane Organization in Photolipid Bilayer Vesicles. *Langmuir.* **34**, 13368–13374 (2018).

[VSF14] Willem A. Velema, Wiktor Szymanski, and Ben L. Feringa. Photopharmacology: beyond proof of principle. *Journal of the American Chemical Society.* **136**, 2178–2191 (2014).

[Whi+76] S. H. White *et al.* Formation of planar bilayer membranes from lipid monolayers. A critique. *Biophys J.* **16**, 481–489 (1976).

[Whi72] S. H. White. Analysis of the torus surrounding planar lipid bilayer membranes. *Biophysical Journal.* **12**, 432–445 (1972).

[Zha+07] Feng Zhang *et al.* Multimodal fast optical interrogation of neural circuitry. *Nature.* **446**, 633–639 (2007).

[Zoc+13] Florian Zocher *et al.* Local partition coefficients govern solute permeability of cholesterol-containing membranes. *Biophys J.* **105**, 2760–2770 (2013).

[Žun+21] Kristina Žuna *et al.* Mitochondrial Uncoupling Proteins (UCP1-UCP3) and Adenine Nucleotide Translocase (ANT1) Enhance the Protonophoric Action of 2,4-Dinitrophenol in Mitochondria and Planar Bilayer Membranes. *Biomolecules.* **11** (2021).

Supplementary Information to

Phototriggered proton-selective carrier currents through photoswitchable membranes

Juergen Pfeffermann[1,a], Rohit Yadav[1,a], Toma Glasnov[2], Oliver Thorn-Seshold[3], Peter Pohl[1]

[1]Institute of Biophysics, Johannes Kepler University Linz, Linz, Austria

[2]Institute of Chemistry, Karl-Franzens-University, Graz, Austria

[3]Faculty of Chemistry and Food Chemistry, Dresden University of Technology, Dresden, Germany

[a]These authors contributed equally: Juergen Pfeffermann and Rohit Yadav.

S1 Negligible background ion permeability

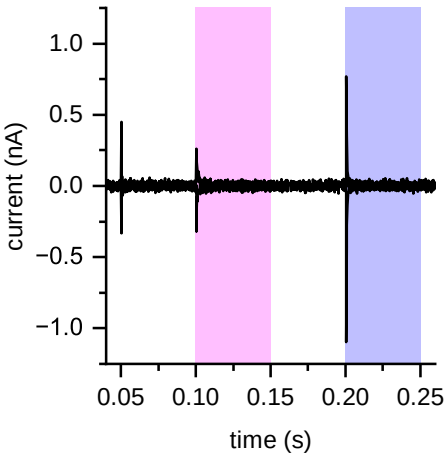

Figure S1: Voltage-clamp current recordings on a 70 µm-diameter photoswitchable PLB (*E. coli* PLE + 20 m% OptoDArG) bathed in 15 mM KCl, 10 mM HEPES pH 7.4. Recordings were made as in Figure 2a (V ranged from 130 mV to −130 mV). Apart from capacitive currents upon voltage application and optocapacitive currents upon light exposure (cf. [Bas+24]), background conductance does not change confoundingly.

In the present study, we were chiefly interested in ion transport mediated by ionophores. In bare lipid bilayers, all other ion transport may be disregarded because of little conductance to inorganic ions [HHP19]. Likewise, the planar lipid bilayer (PLB) model system has a specific resistance of $1 \times 10^6\ \Omega\,\mathrm{cm}^2$ to $1 \times 10^8\ \Omega\,\mathrm{cm}^2$ when unmodified [MM72]. We have previously shown that photoswitchable PLBs containing a mass fraction of up to 20 % OptoDArG retain high resistance [Pfe+21; Bas+24]. Figure S1 shows a voltage-clamp current, I, recording conducted on a photoswitchable PLB folded from *E. coli* PLE + 20 m% OptoDArG following the same protocol used for investigating carrier currents in photoswitchable bilayers (involving voltage steps and alternating laser irradiation with UV and blue light). At $t = 50$ ms a capacitive current transient appears due to the application of voltage. Optocapacitive currents are evident at the onset of light exposure at $t = 100$ ms (UV) and $t = 200$ ms (blue); a detailed description of photolipid photoisomerization-evoked optocapacitive currents is given in [Bas+24]. Apart from these transients, I does not change confoundingly during light exposure. In particular, in the majority of carrier experiments conducted in this study, both background and UV light-activated I are in the nA-range at most voltages. Likewise, irrespective of higher membrane H^+ permeability [HHP19], unfacilitated H^+ currents are orders of magnitude lower than, in particular, light-activated protonophore currents. Hence, for the purposes of this publication, background membrane ion permeability of photoswitchable PLBs in the absence of ionophores can be confidently disregarded.

S2 A basic model of carrier-mediated transmembrane ion transport

Classical carriers are either lipid-soluble ionophores that reversibly bind to specific inorganic ions or weak acids/bases with membrane-permeable charged and neutral forms. By binding the respective ion, they lower the activation energy required for transporting the latter across biological membranes, in particular across their hydrophobic core [Läu72]. Transmembrane ion transport facilitated by ionophores such as valinomycin [HLF95] and CCCP [KBM84] may be described by the basic kinetic scheme shown in Figure 1a [HLF95]. Formally, the carrier is considered to be most of the time in one of four membrane-adsorbed states: ion-dissociated (subscript d) and ion-associated (subscript a) carrier adsorbed to side 1 (superscript $'$) and 2 (superscript $''$) of the membrane, respectively, with associated concentrations N'_d, N'_a, N''_d, and N''_a (units of $\mathrm{mol\,m^{-2}}$). Transitions between these states are characterized by a set of eight rate constants: k'_a, k''_a, k'_d, k''_d are transport rate constants, and k'_A, k''_A, k'_D, k''_D are rate constants of association (subscript A) and dissociation (subscript D) at the interface. Those rates that describe transmembrane movement of the charged species depend on voltage and association/dissociation rate constants may depend on ion concentration at the interface, c_i [HLF95]. Given asymmetric ionic conditions, c'_i and c''_i denote ion concentration at side 1 and 2 of the bilayer, respectively.

Given the kinetic scheme shown in Figure 1a, the simplest expression for the flux of the charged species, J_c, in units of $\mathrm{mol\,m^{-2}\,s^{-1}}$ is given by

$$J_c = k'_c\,N'_c - k''_c\,N''_c \tag{1}$$

and J_c is positive for net flow from side 1 to 2 [HLF95]. The subscript c (read: charged) substitutes for the subscript a or d, depending on which reflects the charged state of the respective carrier. For example, valinomycin is a cationic ionophore and charged when bound to its cargo K^+ whereas CCCP is an anionic protonophore that is charged when deprotonated, i.e., without its cargo H^+. Experimentally, we measure current, I, under voltage-clamp conditions, whereby $V = \Phi_1 - \Phi_2$ is the difference in electrostatic potential between side 1, Φ_1, and side 2, Φ_2, of the bilayer. The following relation holds:

$$I = z\,F\,A_{\mathrm{m}}\,J_{\mathrm{c}} \tag{2}$$

whereby z is valence of the charged species and F is Faraday's constant.

S3 The light-induced increase in valinomycin–K^+ flux is not a result of photooxidation

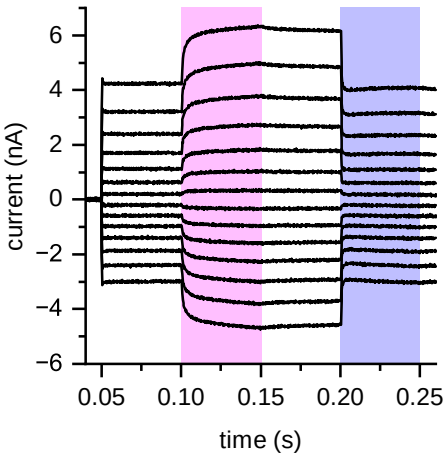

Figure S2: 80 µm-diameter photoswitchable PLB folded from DPhPC + 20 m% OptoDArG with 10 µM valinomycin in 15 mM KCl, 10 mM HEPES pH 7.4. Recordings were made as in Figure 2a.

It is well known that oxidation of unsaturated lipids by the combination of photosensitizer, light and molecular oxygen can permeabilize lipid bilayers [BB19; Fir+23]. Albeit typically disregarded, membrane-targeted light-absorbing compounds can act as photosensitizers, as was shown, for example, in the case of commercial membrane-targeted fluorophores [San+14], molecular motors [Fir+23] and fluorescent membrane tension probes [TCG24]. Besides outright permeabilization, it was suggested that membrane-internal polar oxidation products can favor ion transport, including that of valinomycin–K^+, by an increase in membrane dielectric constant [KS02]. That said, the following speaks against a photodynamic mechanism of action here: (i) azobenzenes are reported to be ineffective at generating singlet oxygen [HMT18]; (ii) the rapid reversibility of the UV light-induced increment in I upon blue light exposure (seen, e.g., in Figure 2a).

In addition to these arguments, we can demonstrate that the increase in valinomycin-mediated I upon UV light exposure also occurs when *E. coli* PLE (containing unsaturated acyl chains) is substituted with the saturated lipid 1,2-diphytanoyl-*sn*-glycero-3-phosphocholine (DPhPC) which is not susceptible to photodynamic damage [RAK93; Fir+23]. The result of an experiment conducted as in Figure 2a but with DPhPC as the main structural lipid is shown in Figure S2. Clearly, the characteristic rapidly-reversible UV light-induced increase in carrier current is maintained. The reduced value of $I_{\mathrm{UV}}/I_{\mathrm{blue}}$ with DPhPC is attributed to differences in bilayer mechanical properties between the natural extract *E. coli* PLE and the synthetic lipid DPhPC with its methyl-branched acyl chains [LPC79]. Notably, OptoDArG photoisomerization in DPhPC-containing photoswitchable PLBs also results in smaller capacitance alterations (data not shown), indicating that membrane geometry is less affected in these membranes (cf. Equation 1). Taken together, rapid reversibility and retention of UV light-induced current increments in saturated bilayers indicates that the observed effect is a result of mechanical alterations to bilayer structure upon photolipid photoisomerization rather than oxidation.

S4 On the potential role of diffusion polarization with NB-lipid at pH 5

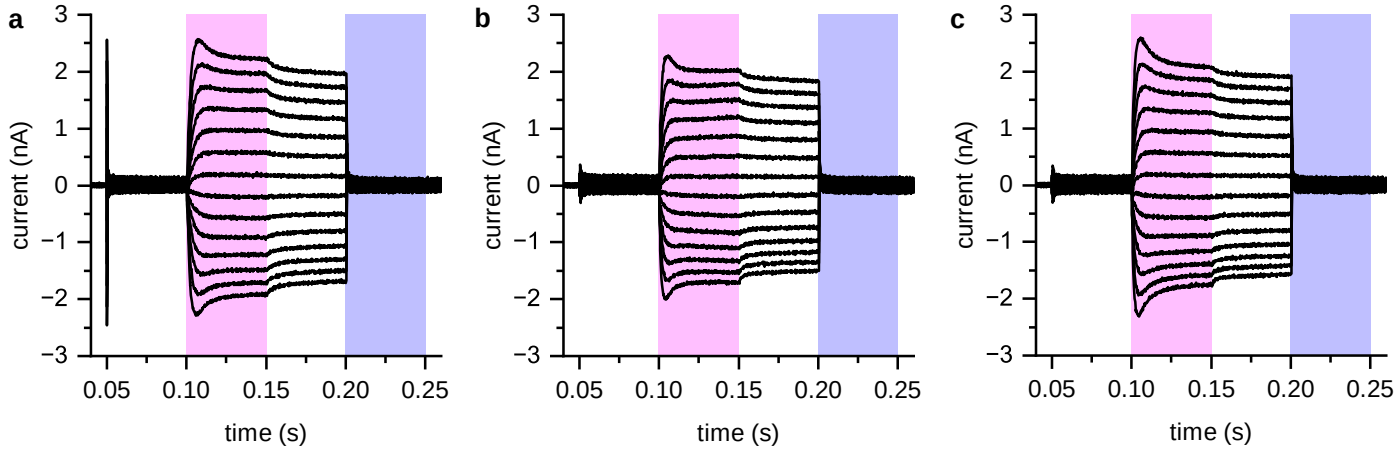

Figure S3: Voltage-clamp current recordings on a 80 µm-diameter photoswitchable PLB folded from *E. coli* PLE + 20 m% OptoDArG + 1 m% NB-lipid in 100 mM KCl, 20 mM MES pH 5. Recordings were made as in Figure 2a. [MES] was 20 mM (panel **a**), 60 mM (panel **b**), and 100 mM (panel **c**). MES was added from a 0.5 M solution adjusted to pH 5.

We observed that, in contrast to valinomycin and CCCP, NB-lipid currents at pH 5 peak and subsequently decrease during constant UV light exposure (Figure 5a). We reasoned that this may be due to diffusion polarization. That is, in the immediate proximity of the PLB, a voltage-driven transmembrane transport of H^+ may have caused an increase in pH in the donating compartment and acidification in the receiving compartment [ADP93]. The resulting $[H^+]$ gradient opposite to the applied voltage may have decreased I. We checked this possibility by increasing buffer capacity, $\mathfrak{B}$, which quantifies the resistance of a buffer solution to a change in pH [US00]. Formally, $\mathfrak{B} = |\mathrm{d}\,c_{\mathrm{a/b}}/\mathrm{d\,pH}|$, whereby $\mathrm{d}\,c_{\mathrm{a/b}}$ is an infinitesimal amount of added acid or base and $\mathrm{d\,pH}$ the ensuing change in pH. Considering monoprotic weak acid buffers (e.g., MES or HEPES) and buffer concentration, c_{B}, in mM (SI-derived unit, $\mathrm{mol\,m^{-3}}$), $\mathfrak{B}$ is given by [Han17]:

$$\mathfrak{B} = \frac{\mathrm{d}\,c_b}{\mathrm{d\,pH}} = -\frac{\mathrm{d}\,c_a}{\mathrm{d\,pH}} = \ln 10 \cdot \left(10^{3-\mathrm{pH}} + 10^{\mathrm{pH}-11} + \frac{[c_{\mathrm{B}}] \cdot 10^{-\mathrm{p}K_{\mathrm{a}}-\mathrm{pH}}}{(10^{-\mathrm{p}K_{\mathrm{a}}} + 10^{-\mathrm{pH}})^2}\right) \tag{3}$$

We repeated the experiment in Figure 5a which which was done at $\mathfrak{B} = 3.2$ mM (20 mM MES at pH 5, $\mathrm{p}K_{\mathrm{a}} = 6.1$ at 25°C [Goo+66]) and subsequently increased [MES] to 60 mM ($\mathfrak{B} = 9.4$ mM) and 100 mM ($\mathfrak{B} = 15.7$ mM). The resulting current recordings, shown in Figure S3, do not differ significantly from each other. Hence, diffusion polarization is not the reason for the peculiar shape of the current traces recorded at pH 5.

S5 Photodynamic modifications of bilayer lipids are not responsible for the observed current modulations

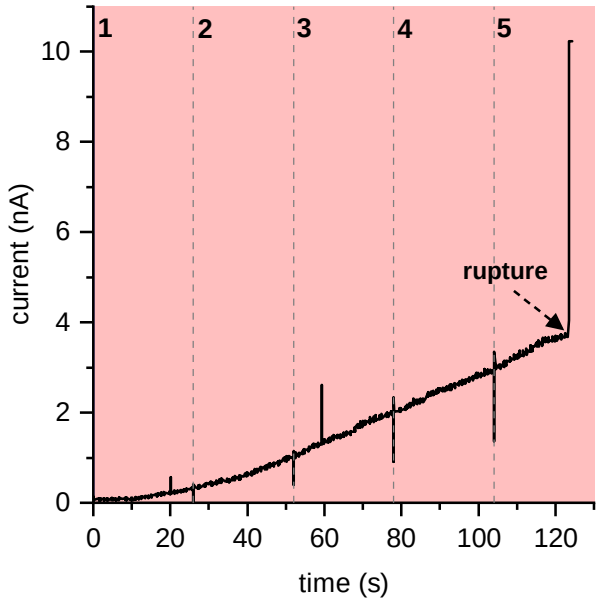

Figure S4: Voltage-clamp current recordings on a PLB folded from *E. coli* PLE + 1 m% NB-lipid bathed in 15 mM KCl, 10 mM HEPES pH 7.4. The applied voltage was $V = 130$ mV. The PLB was constantly exposed to intense red (640 nm) laser light, close to the excitation maximum of nile blue (639 nm [Bau+23]). Five consecutively recorded sweeps, indicated by the dashed vertical lines, are concatenated. Following a gradual increase in conductance, presumably due to photodynamic activity and the accumulation of oxidized lipids, the PLB eventually ruptures, indicated by the arrow.

NB can intercalate in DNA and cause photosensitized DNA damage by electron transfer [Gat+16; Hir+14]. NB can also quantitatively isomerize azobenzenes from cis to trans by a singlet manifold photoredox mechanism, which is particularly effective in NB–azobenzene conjugates [Bau+23]. Indeed, we have observed that OptoDArG can be effectively switched using red light-excited NB-lipid in supramolecular assemblies (publication in preparation). However, the aforementioned observations raise the question whether NB-lipid may photodynamically modify membrane structure (cf. discussion on photosensitized membrane damage in photoswitchable bilayers with valinomycin above). Several facts speak against that: (i) the excitation maximum of NB is at 639 nm, far from the 375 nm used for OptoDArG photoisomerization (yet, absorption spectra can be poor predictors of photochemical reactivity [Irs+21]); (ii) the observed currents are selective for H^+ which may not be the case for oxidative membrane permeabilization; (iii) the UV light-evoked current is rapidly reversible upon blue light exposure (Figure 5ac) – in contrast, photosensitized oxidative damage is not readily reversed by light.

To exclude that the observed UV light-induced current increase is the result of photodynamic membrane modifications, we assessed at which timescale photodynamic effects may be observed. This we tested by voltage-clamp current measurements on a NB-lipid-containing PLB exposed to intense red (640 nm) light. The resulting current trace, shown in Figure S4, qualitatively agrees with literature on photosensitized membrane damage in black lipid membranes [MSS91]: an initial, here relatively short, "induction time" during which I remains constant, followed by a gradual increase in I as a result of the accumulation of photoproducts and eventual membrane rupture. Clearly, tens-of-second long exposure is required to evoke currents in the nA range which still remain smaller than what is achieved within 50 ms of UV light exposure within photoswitchable PLBs (notably, UV and red light irradiance is of comparable magnitude). Hence, considering these vast differences in timescale, we conclude that the observed UV light-induced currents in Figure 5ac are not the result of photodynamic membrane modifications but of changes in membrane material properties upon photoisomerization.

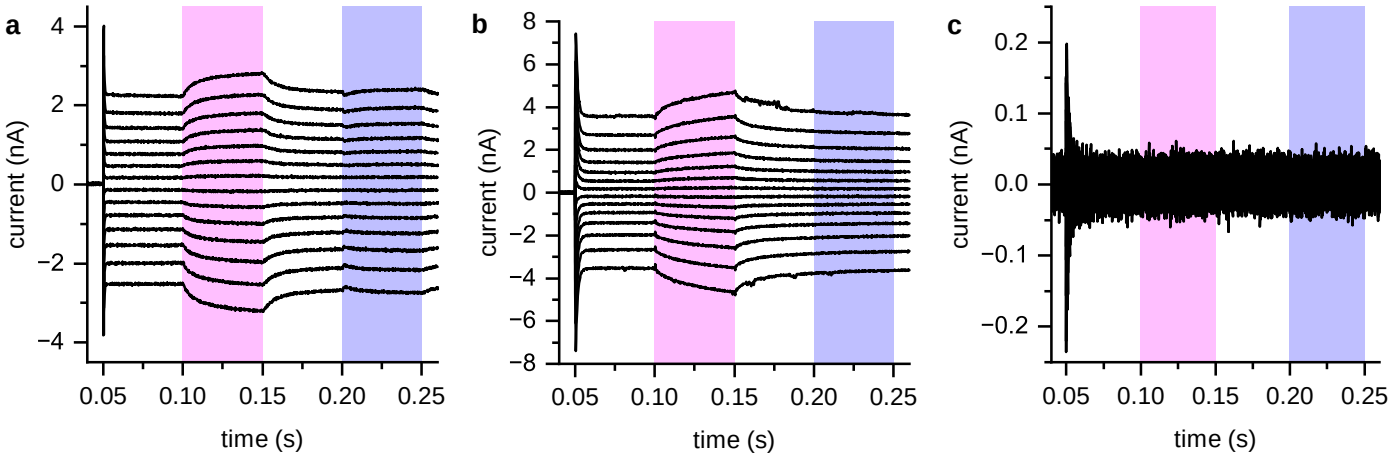

Figure S5: Voltage-clamp current recordings on non-photoswitchable PLBs folded from *E. coli* PLE bathed in 15 mM KCl, 10 mM HEPES pH 7.4 containing nominally 10 µM valinomycin (panel **a**), 10 µM CCCP (panel **b**) or 1 m% NB-lipid (panel **c**). Recordings were made as in Figure 2a.

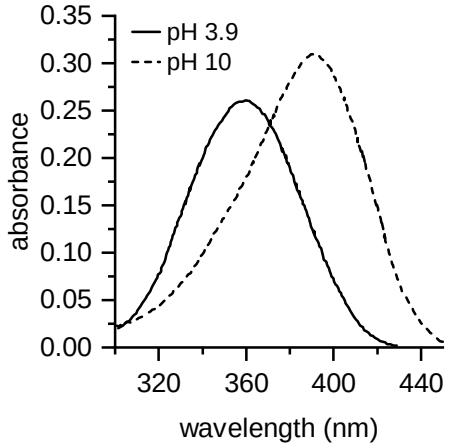

Figure S6: Absorption spectra of 12.5 µM CCCP in the presence of sonicated unilamellar vesicles. The solid line was recorded at pH 3.9, the dashed line at pH 10. Peak absorption wavelengths are at 360 nm (pH 3.9) and 390 nm (pH 10). The data was obtained from Kasianowicz, Benz, and McLaughlin [KBM84] where a detailed description of the measurements can be found.

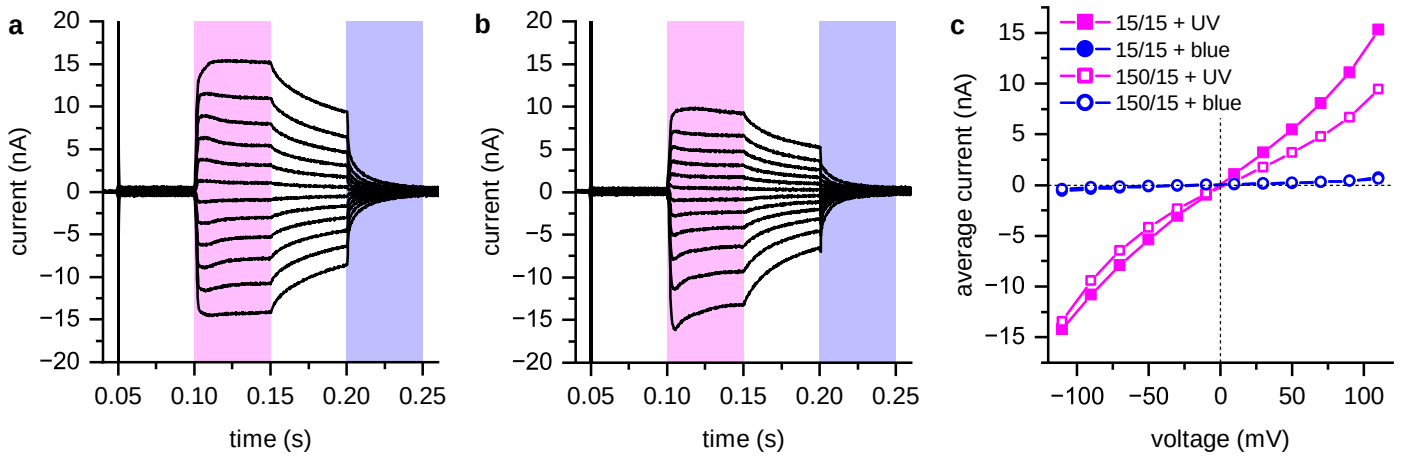

Figure S7: a, Voltage-clamp current recordings on a 85 µm-diameter photoswitchable PLB folded from *E. coli* PLE + 20 m% OptoDArG + 1 m% NB-lipid in 15 mM KCl, 10 mM HEPES pH 7.4. Recordings were made as in Figure 2a with V ranging from 110 mV to −110 mV. **b,** K^+ concentration on side 1 was made 150 mM by the addition of 3 M KCl solution. Recordings were made as in panel **a**. **c,** I/V curves constructed from different intervals of the current traces in panel **a** and **b** as described in Figure 2b.

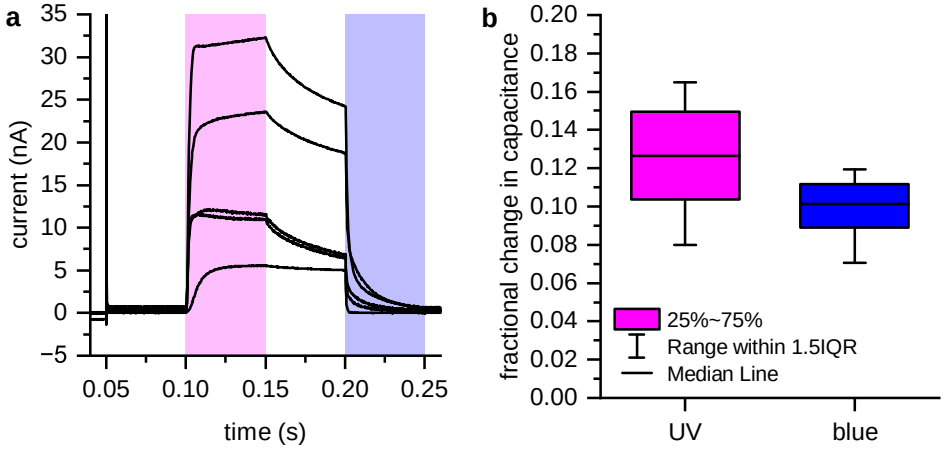

Figure S8: a, Voltage-clamp current recordings on 75 to 95 µm-diameter photoswitchable PLBs folded from *E. coli* PLE + 20 m% OptoDArG + 1 m% NB-lipid in 15 mM KCl, 10 mM HEPES pH 7.4. The traces were recorded in separate measurements which were equally conducted. $V = 90$ mV was applied at $t = 50$ ms. Light exposure as in Figure 2a. **b,** Fractional changes in bilayer capacitance, C_{m}, upon UV and blue light exposure. PLBs were folded from *E. coli* PLE + 20 m% OptoDArG (11 recordings from 3 separate experiments). Capacitance recordings were conducted as described in Figure 2ab in ref. [Bas+24]. Fractional change in capacitance was calculated as $1 - C_{\mathrm{m,peak}}/C_0$ whereby $C_{\mathrm{m,peak}}$ denotes peak capacitance achieved within milliseconds after light exposure and C_0 capacitance immediately before light exposure.

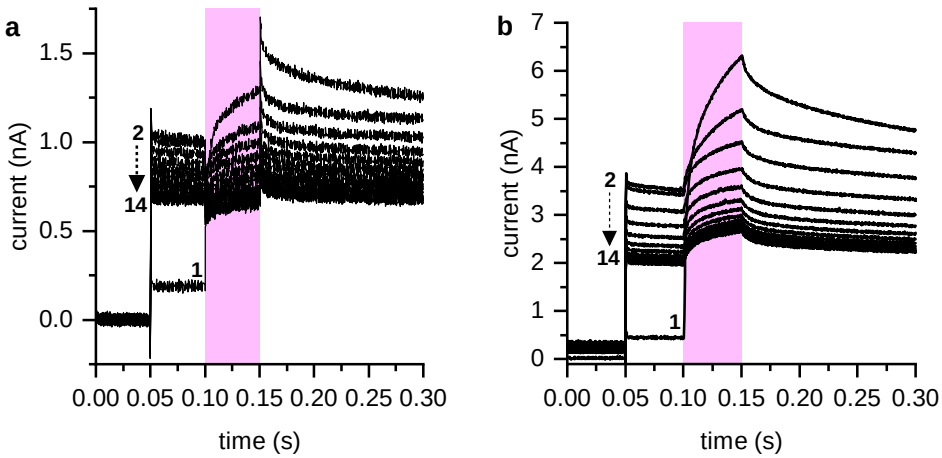

Figure S9: a, Voltage-clamp current recordings on an 85 µm-diameter photoswitchable PLB (*E. coli* PLE + 20 m% OptoDArG) with 2.5 µM CCCP in 15 mM KCl, 10 mM HEPES pH 7.4. Prior to starting the record, the PLB was exposed to blue light to establish the trans photostationary state. The following was repeated 14 times with an intersweep delay of 1 s: Between 0 and 50 ms, $V = 0$ and between 50 and 300 ms, $V = 130$ mV; between 100 and 150 ms the PLB was exposed to UV light (no blue light exposure). **b,** 14 sweeps recorded as in panel **a** on a 77.5 µm-diameter photoswitchable PLB in the presence of 2 µM $[\text{NB-lipid}]_{\text{aq}}$ in 150/15 mM KCl, 10 mM HEPES pH 5/7.4.

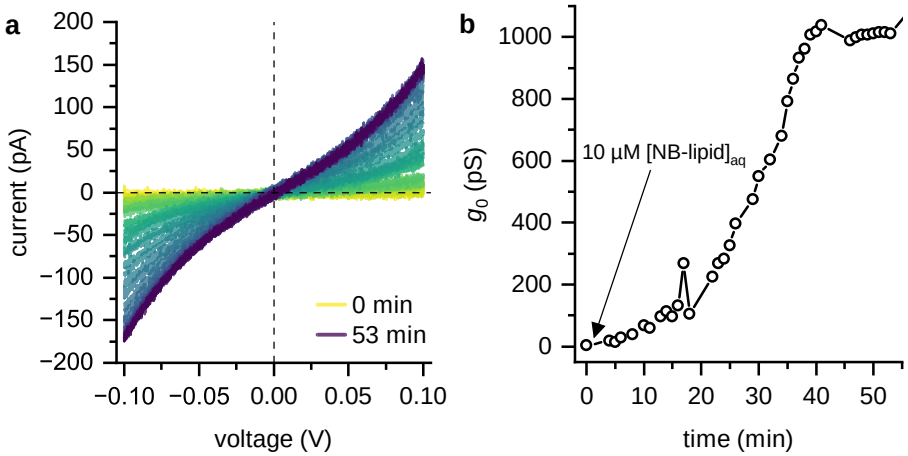

Figure S10: a, Voltage ramps measured as described in Figure 6a on a 135 µm-diameter photoswitchable PLB folded from *E. coli* PLE + 20 m% OptoDArG in 15 mM KCl, 10 mM HEPES pH 7.4. 10 µM [NB-lipid]$_{aq}$ was added to both compartments immediately after the record at $t = 0$ min (yellow line) and further voltage ramps were recorded under continuous stirring for 53 min. **b,** The cubic I/V curves in panel **a** were fit by Equation 5 and the obtained g_0 values are plot over time of record. Conductance increased gradually, indicating slow membrane incorporation of aqueous NB-lipid.

References for the Supplementary Information

[ADP93] Y. N. Antonenko, G. A. Denisov, and P. Pohl. Weak acid transport across bilayer lipid membrane in the presence of buffers. Theoretical and experimental pH profiles in the unstirred layers. *Biophysical Journal.* **64**, 1701–1710 (1993).

[Bas+24] Carlos A. Z. Bassetto *et al.* Photolipid excitation triggers depolarizing optocapacitive currents and action potentials. *Nature Communications.* **15**, 1139 (2024).

[Bau+23] Benedikt Baumgartner *et al.* Azobenzenes can achieve near-infrared photocontrol in biological systems, with quantitative Z→E photoisomerization, via singlet manifold photoredox (2023).

[BB19] Isabel O. L. Bacellar and Mauricio S. Baptista. Mechanisms of Photosensitized Lipid Oxidation and Membrane Permeabilization. *ACS omega.* **4**, 21636–21646 (2019).

[Fir+23] Alexander M. Firsov *et al.* Photodynamic activity rather than drilling causes membrane damage by a light-powered molecular nanomotor. *Journal of photochemistry and photobiology. B, Biology.* **239**, 112633 (2023).

[Gat+16] Hugo Gattuso *et al.* From non-covalent binding to irreversible DNA lesions: nile blue and nile red as photosensitizing agents. *Scientific reports.* **6**, 28480 (2016).

[Goo+66] N. E. Good *et al.* Hydrogen ion buffers for biological research. *Biochemistry.* **5**, 467–477 (1966).

[Han17] Christof Hannesschlaeger. "Transmembrane Diffusion of Poorly Partitioning or Self Inhibiting Solutes". Doctoral Thesis. Johannes Kepler University Linz, 2017.

[HHP19] Christof Hannesschlaeger, Andreas Horner, and Peter Pohl. Intrinsic Membrane Permeability to Small Molecules. *Chem Rev.* **119**, 5922–5953 (2019).

[Hir+14] Kazutaka Hirakawa *et al.* Nile blue can photosensitize DNA damage through electron transfer. *Chemical research in toxicology.* **27**, 649–655 (2014).

[HLF95] S. B. Hladky, J. C. Leung, and W. J. Fitzgerald. The mechanism of ion conduction by valinomycin: analysis of charge pulse responses. *Biophysical Journal.* **69**, 1758–1772 (1995).

[HMT18] Katharina Hüll, Johannes Morstein, and Dirk Trauner. In Vivo Photopharmacology. *Chem Rev.* **118**, 10710–10747 (2018).

[Irs+21] Ishrath Mohamed Irshadeen *et al.* Action Plots in Action: In-Depth Insights into Photochemical Reactivity. *Journal of the American Chemical Society.* **143**, 21113–21126 (2021).

[KBM84] J. Kasianowicz, R. Benz, and S. McLaughlin. The kinetic mechanism by which CCCP (carbonyl cyanide m-chlorophenylhydrazone) transports protons across membranes. *The Journal of membrane biology.* **82**, 179–190 (1984).

[KS02] Frank Killig and Günther Stark. Photodynamic activation of ion transport through lipid membranes and its correlation with an increased dielectric constant of the membrane. *Biochimica Et Biophysica Acta.* **1564**, 207–213 (2002).

[Läu72] P. Läuger. Carrier-mediated ion transport. *Science (New York, N.Y.)* **178**, 24–30 (1972).

[LPC79] H. Lindsey, N. O. Petersen, and S. I. Chan. Physicochemical characterization of 1,2-diphytanoyl-sn-glycero-3-phosphocholine in model membrane systems. *Biochimica Et Biophysica Acta.* **555**, 147–167 (1979).

[MM72] M. Montal and P. Mueller. Formation of bimolecular membranes from lipid monolayers and a study of their electrical properties. *Proc Natl Acad Sci U S A.* **69**, 3561–3566 (1972).

[MSS91] V. M. Mirsky, I. N. Stozhkova, and T. V. Szitó. Photosensitized damage of bilayer lipid membrane in the presence of haematoporphyrin dimethylether. *Journal of photochemistry and photobiology. B, Biology.* **8**, 315–324 (1991).

[Pfe+21] Juergen Pfeffermann *et al.* Photoswitching of model ion channels in lipid bilayers. *Journal of photochemistry and photobiology. B, Biology.* **224**, 112320 (2021).

[RAK93] T. I. Rokitskaya, Y. N. Antonenko, and E. A. Kotova. The interaction of phthalocyanine with planar lipid bilayers. Photodynamic inactivation of gramicidin channels. *FEBS Letters.* **329**, 332–335 (1993).

[San+14] Shalene Sankhagowit *et al.* The dynamics of giant unilamellar vesicle oxidation probed by morphological transitions. *Biochimica Et Biophysica Acta.* **1838**, 2615–2624 (2014).

[TCG24] Joaquim Torra, Felix Campelo, and Maria F. Garcia-Parajo. Tensing Flipper: Photosensitized Manipulation of Membrane Tension, Lipid Phase Separation, and Raft Protein Sorting in Biological Membranes. *Journal of the American Chemical Society.* **146**, 24114–24124 (2024).

[US00] Edward T. Urbansky and Michael R. Schock. Understanding, Deriving, and Computing Buffer Capacity. *Journal of Chemical Education.* **77**, 1640–1644 (2000).